Numerical Analysis of Reinforced Concrete and Steel-Fiber Concrete Elements under Fatigue Loading

Benard Isojeh, Ph.D., P.Eng.[1]; Maria El-Zeghayar, Ph.D.[2]; and Frank J. Vecchio, Ph.D., P.Eng., M.ASCE[3]

Abstract: The implementation of fatigue-damage models into the governing equations of the disturbed stress field model algorithm for fatigue analysis of reinforced concrete structures is presented in this paper. The models account for concrete deterioration, localized reinforcement crack growth, and accumulation of irreversible compressive strain in conventional reinforced concrete and steel-fiber reinforced concrete due to fatigue loading. As such, analyses involving fatigue damage can be expressed in terms of the deformation evolution and residual capacity. These concepts overcome the well-known limitations of stress-life models for fatigue analysis of reinforced concrete structures. The implementation concepts using robust models from the literature are described. As a means of further illustration, the solutions to the deformation of a shear element under pure shear fatigue loading are presented. The validation of the modified algorithm using finite-element analysis with experimental results for fatigue life and residual strength prediction gave good correlation. **DOI: 10.1061/(ASCE)ST.1943-541X.0002349.**

Introduction

A majority of collapsed structures subject to dynamic forces have been linked to component fatigue. This has resulted in the use of fatigue limit-state verification to complement the ultimate and serviceability limit states in the structural design of these structures. As a norm, the fatigue-resistance capacity of a reinforced concrete structure is typically estimated using the stresses induced in the constituent materials obtained from static analyses of the maximum and minimum fatigue loads on the structure. The highest stress values at critical sections are normalized with the ultimate strengths of the materials and are substituted into corresponding fatigue stress-life models (S-N curves) to obtain the number of cycles leading to failure (Aas-Jacobsen 1970).

Experiments conducted and reported in the literature on the fatigue behavior of concrete composites portray progressive deterioration and accumulation of irreversible strains as governing mechanisms. Cracks on reinforcing bars traversing cracked concrete planes have also been observed to evolve to fracture (Lovegrove 1981; Okamura et al. 1981; Zanuy et al. 2009). The inability of S-N models to account for progressive deformation became evident as the need of the damage evolution for concrete after some given number of cycles and load history arose (Holmen 1982).

In order to account for the progressive deformation under fatigue loading, constitutive models were developed for concrete composites and steel reinforcement by various researchers (Otter and Naaman 1986, 1988; Oh 1991; Eligehausen et al. 1992; Park 1990; Gao and Hsu 1998; Teng and Wang 2001; Petryna et al. 2002; Maekawa et al. 2006; Xiang and Zhao 2007; Grebreyouhannes et al. 2008; Vega et al. 1995; Zanuy et al. 2009; Tamulenas et al. 2014). These simplified the prediction of the damage evolution of a structural component up to the instance of collapse due to instability arising from concrete composite degradation and steel reinforcement fracture. However, some constitutive models developed for concrete are based on assumptions not adequately verified experimentally. For example, using a stress-strain relation, the fatigue hysteresis loop of concrete at failure is assumed to intersect the monotonic stress-strain envelope, and the peak stress of a fatigue-damaged concrete element intersects the monotonic stress-strain envelope. Further, the centerlines of the fatigue hysteresis loops are assumed to converge at a common point. Significant fatigue-influencing parameters such as frequency, waveform, and stress ratio, which were neglected, limit the use of such models to structures having similar loading parameters as those used for developing such models (Zhang et al. 1998; Isojeh et al. 2017a).

Although stress-life models (Tilly and Moss 1982; Hanson 1983; JSCE 1986; Petryna et al. 2002) and the Palmgren-Miner rule (linear rule) (Palmgren 1924; Miner 1945) are used in modeling the progressive fatigue degradation of steel reinforcement, it is well-known that crack propagation in steel reinforcement is nonlinear. Because the main region of fatigue failure in reinforced concrete structures typically coincides with the location of concrete cracks intersecting reinforcing bars, the progressive crack-growth of the reinforcement traversing the concrete crack plane should be well-accounted for to appropriately predict the deformation within the concrete plane. Available approaches in the literature that incorporate the stress-life models and Palmgren-Miner rule for steel reinforcement fatigue fracture do not capture this governing fatigue-damage mechanism and its corresponding evolution.

In this paper, robust modified damage models, an irreversible strain model, and constitutive models proposed by Isojeh et al. (2017a, c, d) are used. In addition, the governing fatigue-damage mechanism and local stress conditions at crack locations are adequately accounted for by implementing reinforcement crack-growth models developed from fracture mechanics. These models are incorporated into the monotonic models of the well-known disturbed stress field model (DSFM) as functions of fatigue loading cycles and other salient fatigue-loading parameters; hence, as

[1]Ph.D. Candidate, Dept. of Civil Engineering, Univ. of Toronto, Toronto, ON, Canada M5S 1A4 (corresponding author). Email: mb.isojeh@mail.utoronto.ca

[2]Civil Engineer, Renewable Power Business Unit, Hatch Ltd., 4323 Queen St., Niagara Falls, ON, Canada L2E 2K9.

[3]Professor, Dept. of Civil Engineering, Univ. of Toronto, Toronto, ON, Canada M5S 1A4.

Note. This manuscript was submitted on July 23, 2017; approved on December 6, 2018; published online on August 28, 2019. Discussion period open until January 28, 2020; separate discussions must be submitted for individual papers. This paper is part of the ***Journal of Structural Engineering***, © ASCE, ISSN 0733-9445.

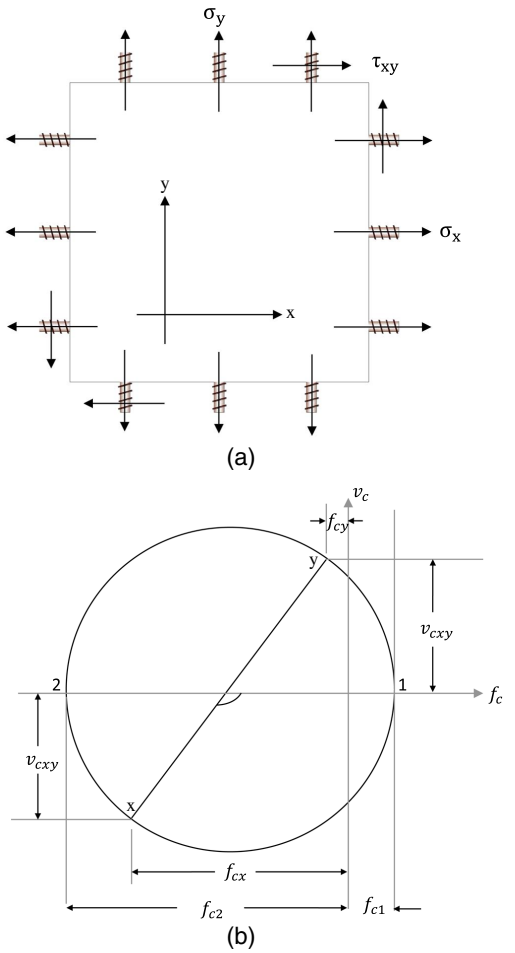

Fig. 1. Steel-fiber reinforced concrete element: (a) loading conditions; and (b) Mohr's circle for average stresses in concrete.

fatigue loading cycles increase, the residual capacity of a structural element and its progressive deformation can be obtained from load-deformation plots and deflection evolutions.

Disturbed Stress Field Model

Solutions to many engineering mechanics problems are obtainable provided associated equilibrium, compatibility, and constitutive equations are satisfied. The capability of DSFM (Vecchio 2000, 2001) to predict the behavior of reinforced concrete structures subjected to different loading conditions is well-documented (Vecchio 2000, 2001; Facconi et al. 2014; Lee et al. 2016). As an extension of the modified compression field theory (Vecchio and Collins 1986), the DSFM, founded on a smeared-rotating crack model, includes the consideration of deformation within concrete crack planes. The formulations of DSFM can be adapted to allow for the consideration of damage of concrete and the corresponding crack growth on steel reinforcement (longitudinal and transverse) intersecting a concrete crack under fatigue loading. The modification of these models is considered subsequently.

Equilibrium Condition

The reaction of an orthogonally reinforced concrete element (Fig. 1) due to external forces will result in induced average stresses in the concrete composite and steel reinforcement. In the cracked state, the verification of equilibrium at the crack locations is required to ensure stresses are adequately transferred between cracks (Fig. 2).

Equilibrium due to Average Stresses

In Fig. 1, the normal stresses are denoted by σ_x and σ_y and the shear stress as τ_{xy}. Considering the average stresses in the element under static loading condition, the equilibrium condition based on the superposition of concrete and steel reinforcement stresses can be expressed as:

$$\sigma_x = f_{cx} + \rho_x f_{sx} \tag{1}$$

$$\sigma_y = f_{cy} + \rho_y f_{sy} \tag{2}$$

$$\tau_{xy} = v_{\text{cxy}} \tag{3}$$

where ρ_x and ρ_y = reinforcement ratios in the x- and y- directions, respectively.

The stresses in the concrete or steel-fiber concrete (f_{cx}, f_{cy}, and v_{cxy}) can be obtained using Mohr's stress circle [Fig. 1(b)] with known principal stresses (f_{c1} and f_{c2}). The principal stresses are obtained from constitutive models, which are functions of concrete parameters such as strength, stiffness, and induced strains. Because these parameters (strength and stiffness) degrade and strains accumulate under fatigue loading, the material stresses change correspondingly. Constitutive models that account for fatigue degradation are considered in a subsequent section.

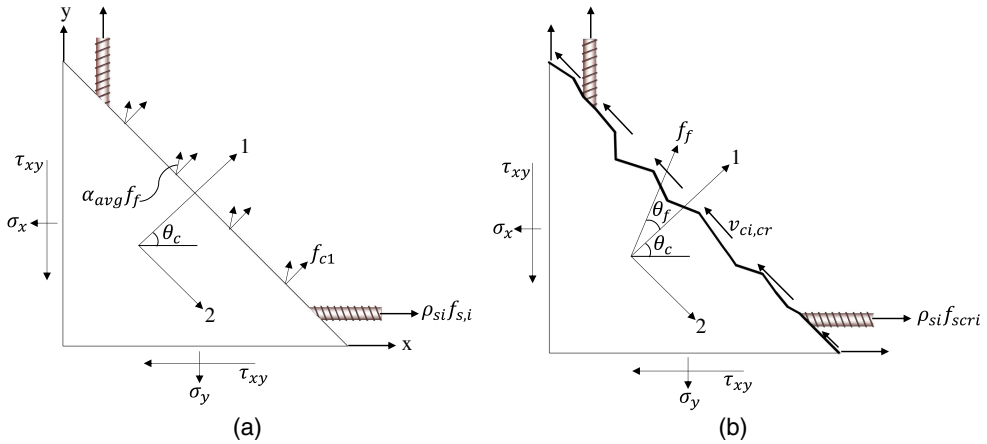

Fig. 2. Equilibrium conditions: (a) parallel to crack direction; and (b) along crack surface.

J. Struct. Eng., 2019, 145(11): 04019126

Equilibrium of Forces at a Crack

Under static loading, stresses in reinforcement at crack locations are higher than the values between cracks (average values) because concrete tensile stress is low or zero at such locations. As a result, shear stresses also develop on the crack surfaces at crack locations.

Because fatigue crack propagation is a function of stress values, its initiation tends to occur at a reinforcement region traversing the concrete cracks where the stresses are high. From Figs. 2(a and b), the general static equilibrium equations that involve steel fiber are given as follows (Lee et al. 2016):

$$f_{c1} = \sum_{i}^{n} \rho_{si}(f_{\text{scri}} - f_{s,i}) \cdot \cos^2\theta_{ni} + (1 - \alpha_{\text{avg}}) f_f \cos\theta_f \quad (4)$$

$$v_{ci,cr} = \sum_{i}^{n} \rho_{si}(f_{\text{scri}} - f_{s,i}) \cdot \cos\theta_{ni} \sin\theta_{ni} - (1 - \alpha_{\text{avg}}) f_f \sin\theta_f \quad (5)$$

where $(1 - \alpha_{\text{avg}})f_f$ = contribution from steel fiber bridging a crack, where α_{avg} relates the tensile stress in the steel fiber to the average principal tensile stress; θ_f = angle between the tensile stress direction due to steel fiber and principal tensile stress direction in concrete; and f_f = function of the equivalent bond strength due to the mechanical anchorage of steel fiber and the friction bond strength of the steel fiber (Lee et al. 2016).

As cracks propagate on the reinforcement traversing a concrete crack, the area of reinforcement intersecting the crack reduces, resulting in a lower reinforcement ratio at the crack. To account for the progressive reinforcement ratio reduction due to fatigue loading, Eqs. (4) and (5) are modified

$$f_{c1} = \sum_{i}^{n} \rho_{si}(Z_O f_{\text{scri}} - f_{s,i}) \cdot \cos^2\theta_{ni} + (1 - \alpha_{\text{avg}}) f_f \sqrt{1 - D_{fc}} \cos\theta_f \quad (6)$$

$$v_{ci,cr} = \sum_{i}^{n} \rho_{si}(Z_O f_{\text{scri}} - f_{s,i}) \cdot \cos\theta_{ni} \sin\theta_{ni} - (1 - \alpha_{\text{avg}}) f_f \sqrt{1 - D_{fc}} \sin\theta_f \quad (7)$$

where Z_O and D_{fc} = parameters representing reinforcement crack growth and plain or steel-fiber concrete strength degradation, respectively.

Reinforcement Crack-Growth Factor (Z_O)

The fractured surface area of a reinforcing bar can be assumed as shown in Fig. 3. The crack depth (a_y) evolves from an initiation point up to the instant when the reserve capacity of the reinforcement at the crack is no longer enough for tensile stress transfer. The definitions for a_y, a_i, and other parameters for obtaining the crack depth at a given fatigue loading cycle have been given by Isojeh and Vecchio (2016).

From Fig. 4, the fractured area $\mathrm{A}(a_y)$ is estimated as follows:

$$\mathrm{A}(a_y) = \frac{\theta_r}{90}\pi r^2 - r\sin\theta_r(2r - a_y) \quad (8)$$

$$\theta_r = \cos^{-1}\left(\frac{r - 0.5a_y}{r}\right) \quad (9)$$

The residual area (A_{res}) of a reinforcing bar after crack propagation to a given number of cycles is obtained as follows:

$$A_{\text{res}} = A_o - \mathrm{A}(a_y) \quad (10)$$

From Eq. (10), the reinforcement crack-growth factor (Z_O) required in Eqs. (6) and (7) is obtained

$$Z_O = \frac{A_{\text{res}}}{A_o} \quad (11)$$

where A_o = cross-sectional area of the uncracked rebar. Z_O is estimated for all reinforcing bars traversing the concrete crack, provided the induced stresses are higher than the threshold value for crack initiation.

Prior to reinforcement crack propagation, the number of cycles resulting in a localized plasticity-crack nucleation or crack initiation may also be included using Masing's model and the Smith-Watson-Topper (SWT) approach [Socie et al. 1984; ASTM STP 1389 (Dowling and Thangjitham 2000)]. To account for this, the value of the reinforcement crack-growth factor is assumed to be a value of 1.0 in Eqs. (6) and (7) until the estimated crack-initiation cycles are reached.

Compatibility Condition

In the disturbed stress field model, the total strain $[\varepsilon]$ in an element consists of the net strain $[\varepsilon_c]$, plastic offset strain $[\varepsilon_c^p]$, elastic offset strain $[\varepsilon_c^o]$, and strain effect due to slip at crack $[\varepsilon_c^s]$. The net strain, which is obtained from the difference between the total strain and other aforementioned strains (generally called prestrains), is required in constitutive models for obtaining average stresses.

As reported in the literature, irreversible strain accumulates under fatigue loading; hence, it can be considered as a prestrain at any given fatigue loading instance. An irreversible fatigue strain model developed by Isojeh et al. (2017c) is used for fatigue prestrain $[\varepsilon_{c,2}^{\text{fat}}]$ in the principal compressive strain direction for conventional and steel-fiber reinforced concrete. The model was developed as a function of residual strength and stiffness damage. These parameters, in turn, are functions of salient factors such as frequency, stress ratio, and fatigue loading cycles. As such, the model is capable of accounting for variations in loading parameters. In the x-y direction, the total strain $[\varepsilon]$ is

$$[\varepsilon] = [\varepsilon_c] + [\varepsilon_c^p] + [\varepsilon_c^o] + [\varepsilon_c^s] + [\varepsilon_c^{\text{fat}}] \quad (12)$$

Total strains are used in the constitutive equations for obtaining steel reinforcement stresses; however, net strains $[\varepsilon_c]$ are required

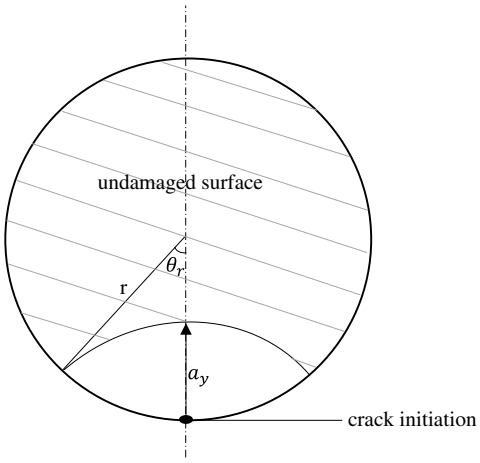

Fig. 3. Crack growth on a reinforcing bar cross section.

in the constitutive models for obtaining average stresses in concrete or steel-fiber concrete. Considering the x-y direction

$$[\varepsilon] = [\varepsilon_x, \varepsilon_y, \gamma_{xy}] \tag{13}$$

$$[\varepsilon_c] = [\varepsilon_{cx}, \varepsilon_{cy}, \gamma_{\mathrm{cxy}}] \tag{14}$$

$$[\varepsilon_c^{\mathrm{fat}}] = [\varepsilon_{cx}^{\mathrm{fat}}, \varepsilon_{cy}^{\mathrm{fat}}, \gamma_{\mathrm{cxy}}^{\mathrm{fat}}] \tag{15}$$

The principal strains (ε_{c1} and ε_{c2}) and the angle of inclination can be estimated from Mohr's circle of strain. Isojeh et al. (2017c) developed the following:

$$\varepsilon_{c,2}^{\mathrm{fat}} = \varepsilon_{do} + \varepsilon_{d1} + \varepsilon_{d2} \tag{16}$$

$$\varepsilon_{do} = -\left(\frac{f_c' + (\sigma_{\max} R)}{E}\right) - 0.3\varepsilon_c' \tag{17}$$

$$\varepsilon_{d1} = k_2 q \left(\frac{D_{fc}}{\sqrt{D_{ce}}}\right) \tag{18}$$

$$\varepsilon_{d2} = \frac{(\sigma_{\max} R)}{E_{\mathrm{sec}}} \tag{19}$$

where E = fatigue secant modulus; $k_2 = 1.0$ for high-strength concrete and 2.0 for normal-strength concrete; q in Eq. (18) = $-0.3\varepsilon_c'$; R = stress ratio; $\sigma_{\max}$ = maximum stress level; and E_{sec} = residual static secant modulus. The models for D_{fc} (concrete strength damage) and D_{ce} (fatigue secant modulus damage) are given in a subsequent section.

Constitutive Relation

The behavior of cracked concrete in compression and the corresponding influences of transverse stresses and shear-slip effects under static loading have been well illustrated by Vecchio (2000). Constitutive models for plain and steel-fiber reinforced concrete are usually given in terms of peak stresses and corresponding strains at peak stresses. Models proposed by Hognestad (1957) and Popovics (1973) for normal and high-strength concrete, respectively, were modified by Isojeh et al. (2017c, d) to account for concrete deterioration and are presented herein for fatigue constitutive relation. The modified Hognestad's equation for fatigue damage is expressed in Eqs. (20)–(22). The residual strength damage (D_{fc}) in the equations will be considered shortly

$$f_c^* = (1 - D_{fc}) f_p \tag{20}$$

$$\varepsilon_c^* = \varepsilon_p (1 + \sqrt{D_{fc}}) - \varepsilon_d \tag{21}$$

where f_c^* = degraded compressive strength; f_p = compressive strength of concrete; and ε_c^* = strain corresponding to the degraded concrete's compressive strength.

The effective stress in fatigue-damaged concrete is

$$f_{c2} = f_c^* \left(\frac{2\varepsilon_{c2}}{\varepsilon_c^*} - \left(\frac{\varepsilon_{c2}}{\varepsilon_c^*}\right)^2\right) \tag{22}$$

For high-strength plain concrete ($f_p \geq 40$ MPa) [using the Popovics (1973) equation], the fatigue constitutive equation is given in a simplified form as follows:

$$f_{c2} = f_p (1 - D_{fc}) \frac{\left(\frac{n\varepsilon_{c2}}{\varepsilon_{\mathrm{p}}}\right)}{(n-1) + (\varepsilon_{c2}/\varepsilon_{\mathrm{p}})^{nk}} \tag{23}$$

where according to Collins and Mitchell (1997)

$$n = 0.80 - f_p/17 \ (\mathrm{MPa}) \tag{24}$$

$$k = 0.6 - \frac{f_p}{62} \quad \text{for } \varepsilon_{c2} < \varepsilon_p < 0 \tag{25}$$

$$k = 1 \quad \text{for } \varepsilon_{c2} < \varepsilon_p < 0 \tag{26}$$

For steel-fiber concrete, the monotonic constitutive model proposed by Lee et al. (2016) was modified to account for fatigue damage

$$f_{c2} = f_{c2\max}(1 - D_{fc}) \left[\frac{A(\varepsilon_{c2}/\varepsilon_{\mathrm{p}})}{A - 1 + (\varepsilon_{c2}/\varepsilon_{\mathrm{p}})^B}\right] \tag{27}$$

$$f_{c2\max} = \frac{f_c'}{1 + 0.19(-\varepsilon_{c1}/\varepsilon_{c2} - 0.28)^{0.8}} < f_c' \tag{28}$$

The values for A and B differ for the hardening and softening portion of the stress-strain envelope. From Lee et al. (2016), the values are as follows:

For the prepeak ascending branch

$$A = B = 1/[1 - (f_c'/\varepsilon_c' E_c)]$$

For postpeak

$$A = 1 + 0.723(V_f l_f/d_f)^{-0.957};$$

$$B = \left(\frac{f_c'}{50}\right)^{0.064} [1 + 0.882(V_f l_f/d_f (V_f l_f/d_f)^{-0.882}]$$

The residual strength damage evolution model is given in Eq. (29) (Isojeh et al. 2017a). The damage parameter in the equation depends on the steel-fiber volume and can be obtained from Fig. 4

$$D_{fc} = D_{cr} \mathrm{Exp}\left[s\left(\frac{\Delta f}{f_c'} - u\right)\right] N^v \tag{29}$$

$$\mathrm{u} = C_f(1 - \gamma_2 \log(\zeta N_f T)) \tag{30}$$

$$\mathrm{v} = 0.434 \ \mathrm{s}\, C_f(\beta_2(1 - R)) \tag{31}$$

where D_{cr} = critical damage value, which is taken as 0.35 and 0.4 for strength and elastic modulus, respectively; C_f = frequency factor; and γ_2, and β_2 = material constants, which are given, respectively, as follows (Zhang et al. 1996):

$$C_f = ab^{-\log f} + c \tag{32}$$

$$\gamma_2 = 2.47 \times 10^{-2}, \qquad \gamma_2 = 0 \quad (\text{for steel fiber})$$

$$\beta_2 = 0.0661 - 0.0226R \tag{33}$$

where for steel-fiber concrete, $\beta_2 = 0.0588$ and 0.0470 for a steel fiber volume of 0.75% and 1.5%, respectively (Isojeh et al. 2017d); a, b, and $c = 0.249$, 0.920, and 0.796 for plain concrete (Zhang et al. 1996) and 0.283, 0.941, and 0.715, respectively, for steel-fiber concrete (Isojeh et al. 2017d); ζ = dimensionless coefficient, which is taken as 0.15 for a sinusoidal cycle (Zhang et al. 1998; Torrenti et al. 2010); and f = fatigue loading frequency.

The behavior of cracked concrete has been considered so far. In an uncracked element, a linear relation for concrete in tension is modified

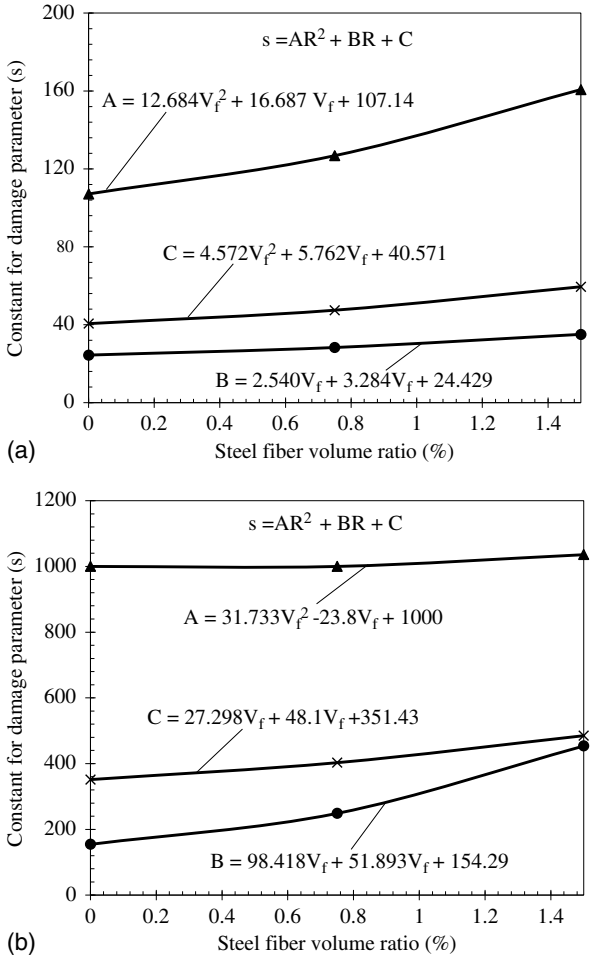

Fig. 4. Damage parameter s for (a) steel-fiber secant modulus; and (b) residual strength.

$$f_{c1} = E_c(1 - D_{te})\varepsilon_{c1} \tag{34}$$

where f_{c1} = tensile stress in the concrete; E_c = initial tangential modulus; and ε_{c1} = principal tensile strain in the concrete. Compressive fatigue damage in an uncracked concrete element is generally considered insignificant because the induced compressive stress is usually small.

Because of bonding between concrete and steel reinforcement, which results in load transfer between the concrete and reinforcement, tension stiffening is usually considered under monotonic loading [Eq. (35)]. Under fatigue loading, however, the effect reduces progressively due to the evolving tensile strain in cracked concrete and reinforcement crack propagation.

The coefficient c_f accounts for the influence of steel fiber (end-hooked) (Lee et al. 2013)

$$f_{c,\mathrm{TS}} = \frac{f_{tp}}{1 + \sqrt{3.6c_f \cdot \varepsilon_{c1}}} \tag{35}$$

where $c_f = 0.6 + (1/0.034)(l_f/d_f)[(100V_f)^{1.5}/M^{0.8}]$, where M is a bond parameter equal to $A_c/(\sum d_{b,i}\pi)$ (mm). For plain concrete, the value of c_f is taken as 0.6. The tensile stress in steel-fiber concrete is estimated as the sum of the tension stiffening effect and stresses transmitted by the steel fiber across cracks

$$f_{c1} = f_{c,\mathrm{TS}} + (1 - \alpha_{\mathrm{avg}})f_f \cos\theta_f \tag{36}$$

where $d_{b,i}$ = rebar diameter. The second term in Eq. (36) is null in the case of conventional reinforced concrete.

The tensile stress in Eq. (36) is required to be less or equal to the right-hand side of Eq. (6). Further, the crack-spacing model proposed by Deluce et al. (2014) is used to relate crack width to average tensile strain, and the shear-slip model proposed by Vecchio and Lai (2004) is used to estimate the slip prestrain and deviation of steel-fiber tensile stress. The models are given subsequently.

For steel-fiber concrete

$$S_{cr} = 2\left(c_a + \frac{s_b}{10}\right)k_3 + \frac{k_1 k_2}{s_{mi}} \tag{37}$$

where S_{cr} = average crack spacing; $c_a = 1.5a_{gg}$; $k_1 = 0.4$; $k_2 = 0.25$; and $k_3 = 1 - [\min(V_f, 0.015)/0.015][1 - (1/k_f)]$, where a_{gg} is the maximum aggregate size (mm) and

$$s_b = \frac{1}{\sqrt{\sum_i \frac{4}{\pi}\frac{\rho_{s,i}}{d_{b,i}^2}\cos^4\theta_i}} \tag{38}$$

$$s_{m,i} = \sum_i \frac{\rho_{s,i}}{d_{b,i}}\cos^2\theta_i + k_f\frac{\alpha_f V_f}{d_f} \tag{39}$$

For conventional reinforced concrete, $S_{cr} = 1/(|\cos\theta|/s_{mx} + |\sin\theta|/s_{my})$, and

$$\delta_s = \delta_2\sqrt{\frac{\psi}{1 - \psi}} \tag{40}$$

$$\delta_2 = \frac{0.5v_{c\max} + v_{co}}{1.8w_{cr}^{-0.8} + (0.234w_{cr}^{-0.707} - 0.20)f_{cc}} \tag{41}$$

where δ_s = crack slip; s_{mx} and s_{my} = average crack spacing in the x- and y-directions, respectively; k_f = factor accounting for the steel-fiber aspect ratio; $\psi = v_{ci,cr}/v_{c\max}$; $v_{c\max} = \sqrt{f'_c}/[0.31 + (24(w_{cr}/a_{gg}) + 16)$ (MPa); $v_{co} = f_{cc}/30$; f_{cc} = concrete cube strength (MPa); and $w_{cr} = S_{cr}\varepsilon_{c1}$. For conventional reinforced concrete, δ_s is taken as δ_2, but the numerator is replaced with shear stress $v_{ci,cr}$ for conventional reinforced concrete [Eq. (7)].

The shear strain resulting from the crack slip is estimated as $\gamma_s = \delta_s/s$ and resolved into x- and y-components

$$\varepsilon_x^s = -\gamma_s/2 \cdot \sin 2\theta \tag{42}$$

$$\varepsilon_y^s = \gamma_s/2 \cdot \sin 2\theta \tag{43}$$

$$\gamma_{xy}^s = -\gamma_s/2 \cdot \cos 2\theta \tag{44}$$

Because shear stresses and slip are functions of the reinforcement ratio or progressing principal stresses, their corresponding values evolve. The tensile stress resulting from steel-fiber bridging deviates by an angle θ_f from the direction of the principal tensile stress (f_{c1}). This deviation angle, according to Lee et al. (2016), is estimated

$$\theta_f = \tan^{-1}\frac{\delta_s}{w_{cr}} \tag{45}$$

Conventional Reinforcement

Although a trilinear stress-strain relation is used to model the response of reinforcement in the disturbed stress field model, a

bilinear stress-strain relation (elastic-perfectly plastic) may be used for fatigue analysis.

Finite-Element Implementation

After each fatigue loading cycle, a structural element may exhibit some level of damage. The response of the structural element per fatigue loading cycle can be obtained. The general formulation of a material stiffness matrix is

$$[\sigma] = [D][\varepsilon] - [\sigma^o] \tag{46}$$

where $\{\sigma\}$ and $\{\varepsilon\}$ are total stress and total strain vectors due to the applied maximum fatigue load (ratio of the minimum to maximum fatigue loading is a parameter required in a subsequent section); and $[D]$ is the transformed composite stiffness matrix, which may degrade due to fatigue loading. Normal and shear stresses on an element are given by

$$\{\sigma\} = \begin{bmatrix} \sigma_x \\ \sigma_y \\ \tau_{xy} \end{bmatrix} \tag{47}$$

Eq. (48) gives the corresponding strain values

$$\{\varepsilon\} = \begin{bmatrix} \varepsilon_x \\ \varepsilon_y \\ \gamma_{xy} \end{bmatrix} \tag{48}$$

$$[D] = [D_c] + \sum_{i=1}^{n} [D_s]_i + [D_f] \tag{49}$$

Prior to cracking

$$[D_c] = \frac{E_c(1 - D_{te})}{1 - \nu^2} \begin{bmatrix} 1 & \frac{\nu}{(1 - D_{te})} & 0 \\ \nu & \frac{1}{(1 - D_{te})} & 0 \\ 0 & 0 & \frac{1 - \nu}{2(1 - D_{te})} \end{bmatrix} \tag{50}$$

where D_{te} = concrete tensile strength damage and is obtained using Eqs. (29)–(31). However, Δf and f_c' are replaced with the induced tensile stress and tensile strength of concrete, respectively. For a given element strain condition, normal stresses in concrete can be found, and subsequently, the principal tensile and compressive stresses and principal strain direction can be obtained.

For a two-dimensional cracked state, the stiffness of concrete with respect to axes of orthotropy, the stiffness of steel reinforcement with respect to its direction, and the stiffness of steel fiber with respect to the inclination of tensile stress due to the steel fiber are all required [Eqs. (51)–(53)]. Subsequently, the stiffnesses are transformed back to reference x- and y-axes [Eq. (54)]

$$[D_c]' = \begin{bmatrix} \overline{E_{c1}} & 0 & 0 \\ 0 & \overline{E_{c2}} & 0 \\ 0 & 0 & \overline{G_c} \end{bmatrix} \text{ for concrete} \tag{51}$$

$$\overline{E_{c1}} = f_{c1}/\varepsilon_{c1}; \qquad \overline{E_{c2}} = f_{c2}/\varepsilon_{c2}; \quad \text{and}$$
$$\overline{G_c} = \overline{E_{c1}} \cdot \overline{E_{c2}}/(\overline{E_{c1}} + \overline{E_{c2}})$$

$$[D_s]_i' = \begin{bmatrix} \rho_i \overline{E_{si}} & 0 & 0 \\ 0 & 0 & 0 \\ 0 & 0 & 0 \end{bmatrix} \text{ for steel reinforcement} \tag{52}$$

$$\overline{E_{s,i}} = f_{s,i}/\varepsilon_{s,i}$$

$$[D_f]' = \begin{bmatrix} \rho_i \overline{E_{f1}} & 0 & 0 \\ 0 & 0 & 0 \\ 0 & 0 & 0 \end{bmatrix} \text{ for steel fiber} \tag{53}$$

$$\overline{E_{f1}} = \alpha_{\text{avg}} f_f/\varepsilon_{cf};$$
$$\varepsilon_{cf} = (\varepsilon_{c1} + \varepsilon_{c2})/2 + [(\varepsilon_{c1} - \varepsilon_{c2})/2]\cos 2\theta_f$$

$$[D_c] = [T_c]^T [D_c]' [T_c];$$
$$[D_f] = [T_f]^T [D_f]' [T_f];$$
$$[D_{s,i}] = [T_{s,i}]^T [D_{s,i}]' [T_{s,i}] \tag{54}$$

$$[T] = \begin{bmatrix} \cos^2\psi & \sin^2\psi & \cos\psi \sin\psi \\ \sin^2\psi & \cos^2\psi & -\cos\psi \sin\psi \\ -2\cos\psi \sin\psi & 2\cos\psi \sin\psi & (\cos^2\psi - \sin^2\psi) \end{bmatrix} \tag{55}$$

For concrete, $\psi = \theta_c$; for steel fiber, $\psi = \theta_c + \theta_f$; and for the steel reinforcing bar, $\psi = \alpha_i$. $[\sigma^o]$ is estimated as a pseudoload using Eqs. (12)–(19) (in this case, it is assumed that there are no prestrains in steel reinforcement)

$$[\sigma^o] = [D_c]([\varepsilon_c^p] + [\varepsilon_c^o] + [\varepsilon_c^s] + [\varepsilon_c^{\text{fat}}]) \tag{56}$$

Subsequently, the total strain can be estimated

$$[\varepsilon] = [D]^{-1}([\sigma] + [\sigma^o]) \tag{57}$$

For further exemplification on the procedure for fatigue analysis of a reinforced concrete element, a flowchart is shown in Fig. 5.

The solution to the fatigue analysis of a shear panel is illustrated using the flow chart given in Fig. 5 in a stepwise manner. Three different pure shear fatigue loads (Fig. 6) (3.5, 3, and 2.7 MPa) were used, and the corresponding deformation evolutions of the material parameters were obtained.

From an initial static analysis using the disturbed stress field model (Vecchio 2000, 2001), the average stresses induced in concrete and steel reinforcement are estimated. Under fatigue loading cycles, the estimated stresses from the static analysis and a chosen number of fatigue loading cycles are substituted into the corresponding fatigue-damage models (A, B, and C in Fig. 5) to obtain the required values for the irreversible strain, concrete strength damage, and steel reinforcement crack depth corresponding to the chosen fatigue loading cycles. At this juncture, it is worth reiterating that the damage models used account for fatigue loading parameters (frequency, waveform, and stress ratio). The properties of the shear panel are:

$$f_c' = 19.0 \text{ MPa}; \qquad \rho_x = 1.785\%$$

$$f_t' = 1.72 \text{ MPa}; \qquad \rho_y = 0.713\%$$

$$\varepsilon_c' = -2.15 \times 10^{-3}; \qquad f_{yx} = 458 \text{ MPa}$$

$$f_{yy} = 300 \text{ MPa}$$

$$E_s = 200{,}000 \text{ MPa}$$

$$a = 10 \text{ mm}$$

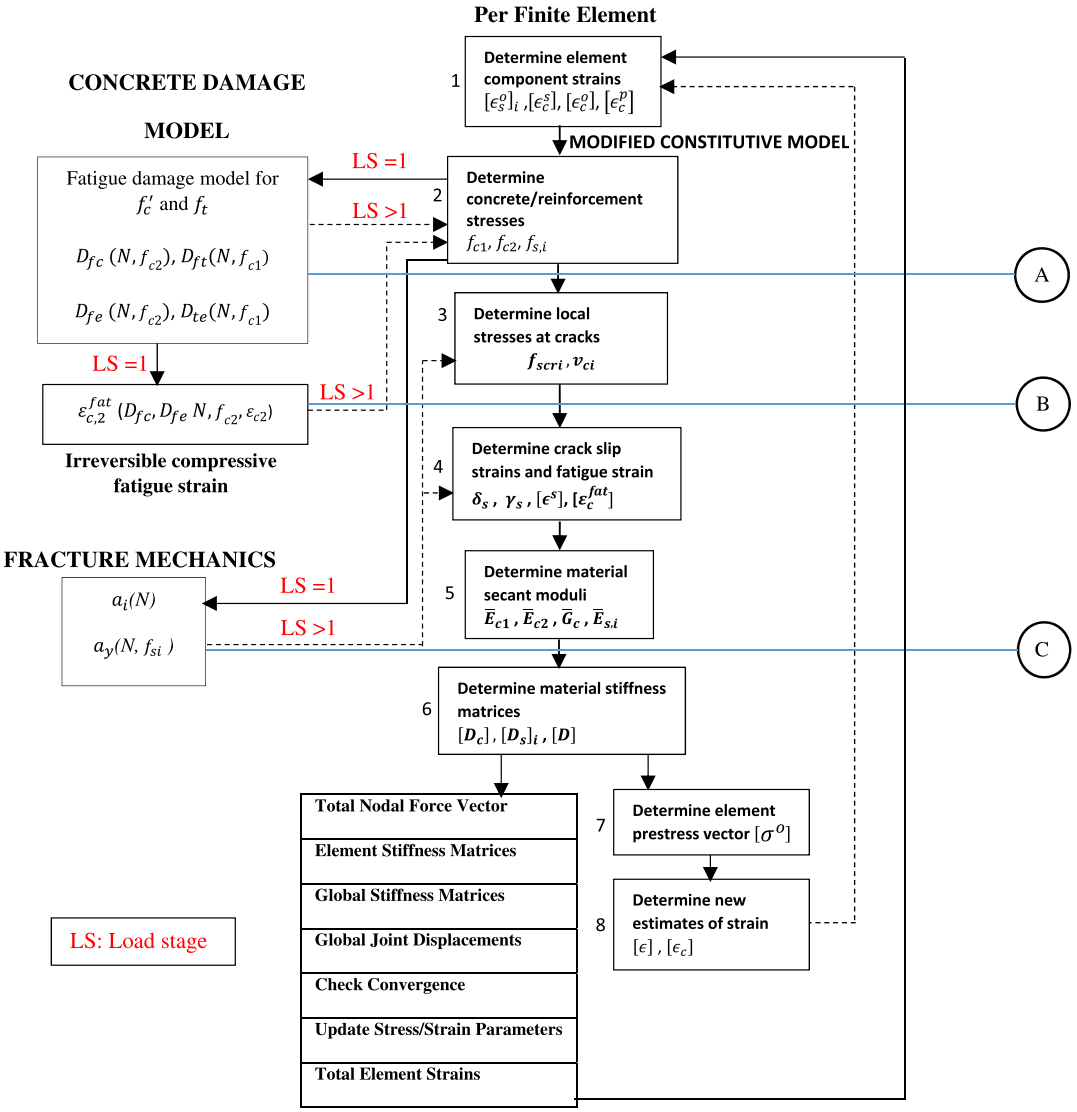

Fig. 5. Flowchart for the modified solution algorithm for DSFM.

$$s_x \approx 50 \text{ mm}; \qquad d_{bx} \approx 6.35 \text{ mm}$$

$$s_y \approx 50 \text{ mm}; \qquad d_{by} \approx 4.01 \text{ mm}$$

$$\text{Fatigue frequency} = 5\text{-Hz waveform} = \text{sinusoidal}$$

$$\text{Load ratio } (R) = 0$$

$$[\sigma] = \begin{bmatrix} 0 \\ 0 \\ 3 \end{bmatrix} \text{ MPa}$$

where f_t', f_{yx}, and f_{yy} = tensile strength of concrete, yield strength of rebars in the x-direction, and yield strength of rebars in the y-direction, respectively.

Solution

The assumed initial total and net strains (from previous calculations) for an applied shear stress of 3 MPa on the shear element in Fig. 6

$$\{\varepsilon\} = \begin{bmatrix} 0.431 \\ 0.792 \\ 1.725 \end{bmatrix} \times 10^{-3}; \qquad \{\varepsilon_c\} = \begin{bmatrix} 0.566 \\ 0.659 \\ 1.716 \end{bmatrix} \times 10^{-3}$$

Using an iterative process, the monotonic response (stress and strain values) due to an applied fatigue load (3 MPa) is obtained.

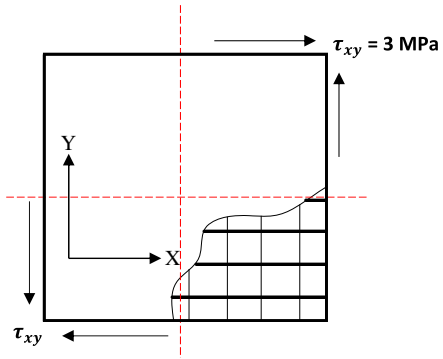

Fig. 6. Shear panel (PV19).

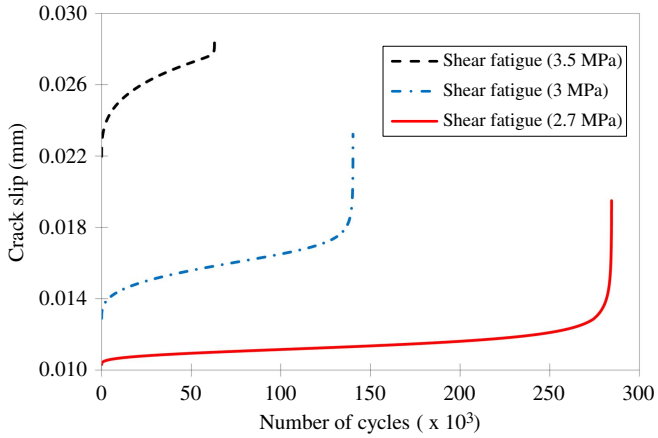

Fig. 7. Crack slip evolution.

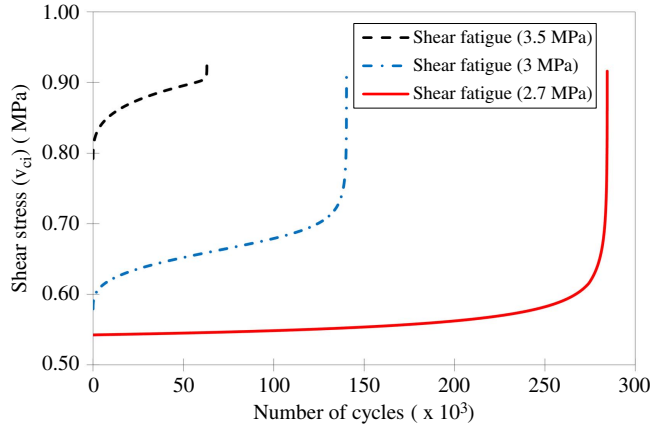

Fig. 8. Shear-stress evolution at crack.

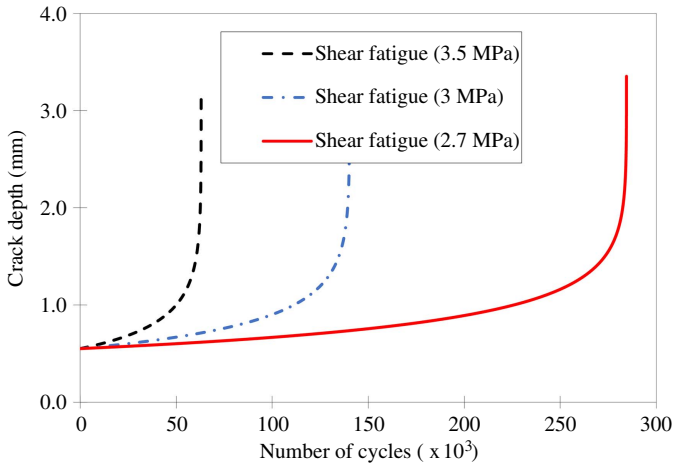

Fig. 9. Reinforcement (y-direction) crack-growth depth.

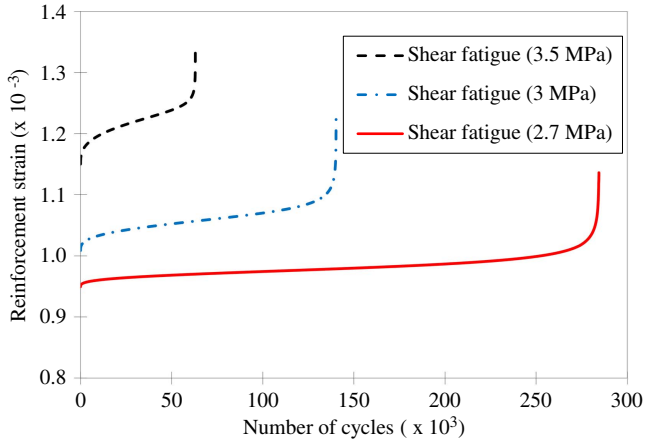

Fig. 10. Reinforcement (x-direction) strain evolution at crack location.

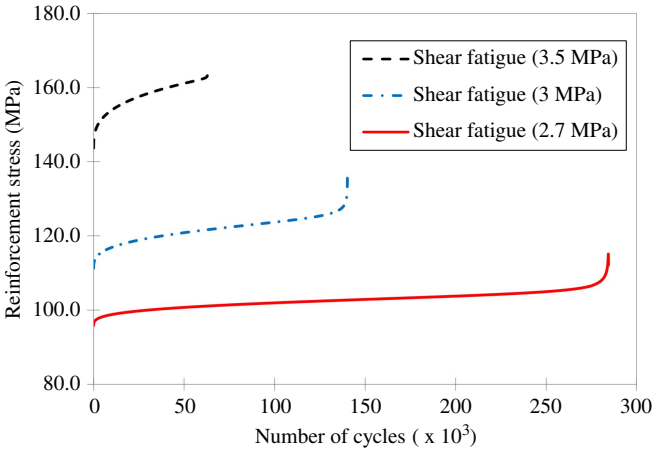

Fig. 11. Reinforcement (x-direction) average stress evolution.

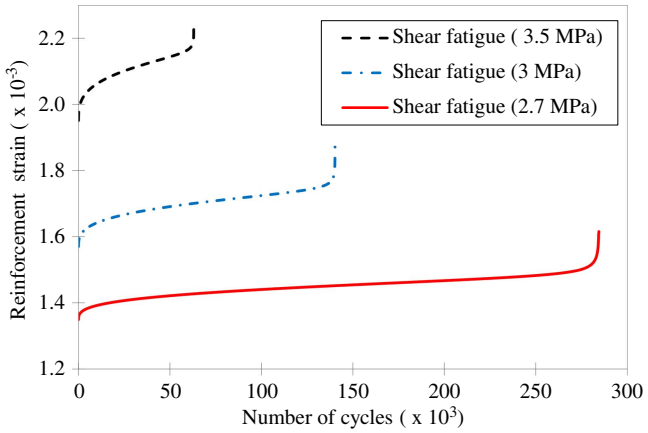

Fig. 12. Localized reinforcement strain evolution (y-direction).

The contribution of the fatigue-damage values (A, B, and C) is neglected for the monotonic analysis.

The initial total and net strains are always replaced by the values estimated in Box 8 (Fig. 5). This continues until the initial values are equal to the final values obtained in Box 8 (Fig. 5).

The obtained element stresses due to the monotonic response are thus $f_{sx} = 111$ MPa and $f_{sy} = 241$ MPa (both stresses are required in the fracture mechanics model). In addition, $f_{c2} = -5.35$ MPa and $f_{c1} = 1.08$ MPa (required in concrete damage model and irreversible strain model). These values are substituted into A, B, and C in Fig. 5 to estimate the corresponding damage at

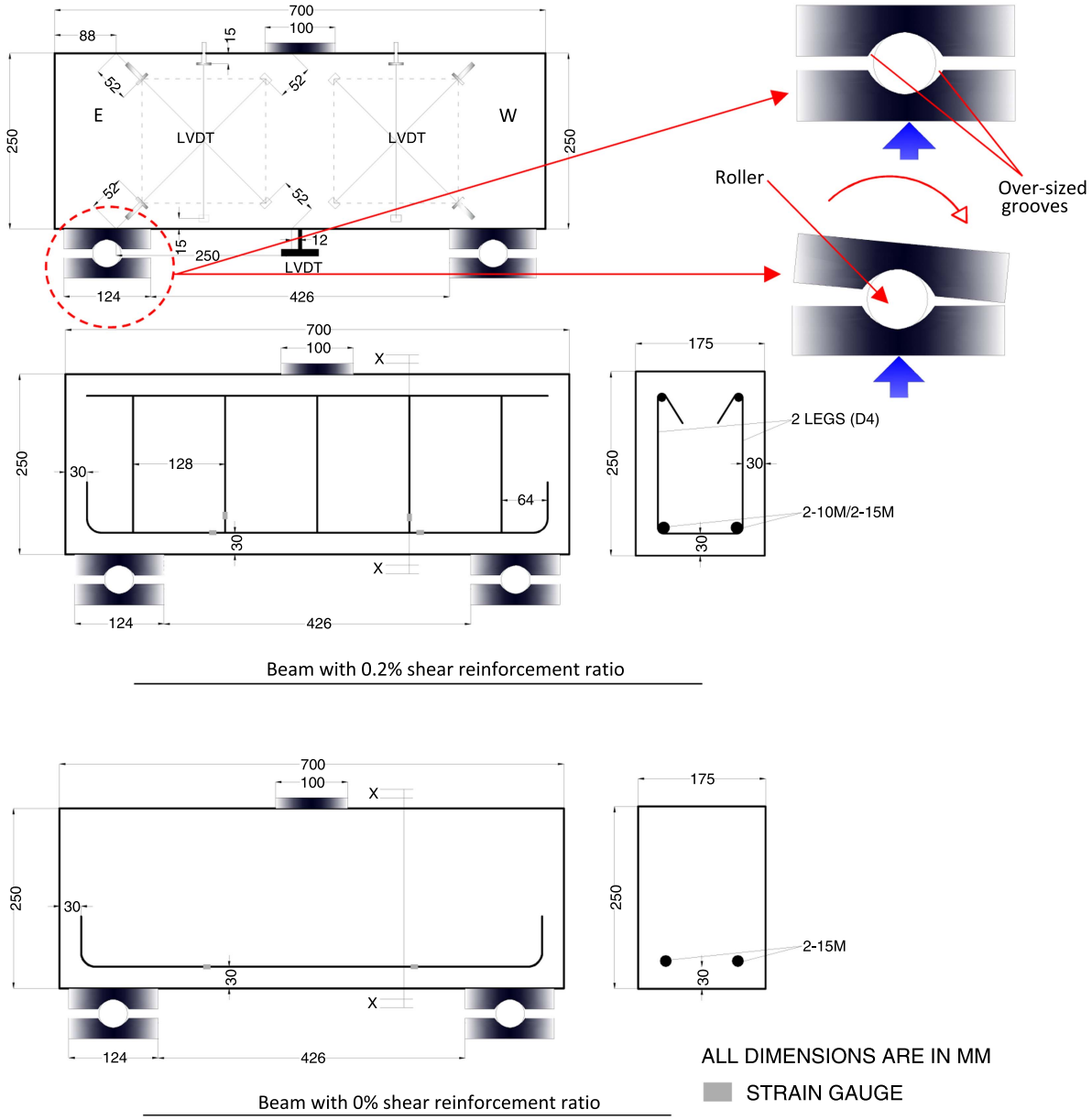

Fig. 13. Details of deep beam specimen.

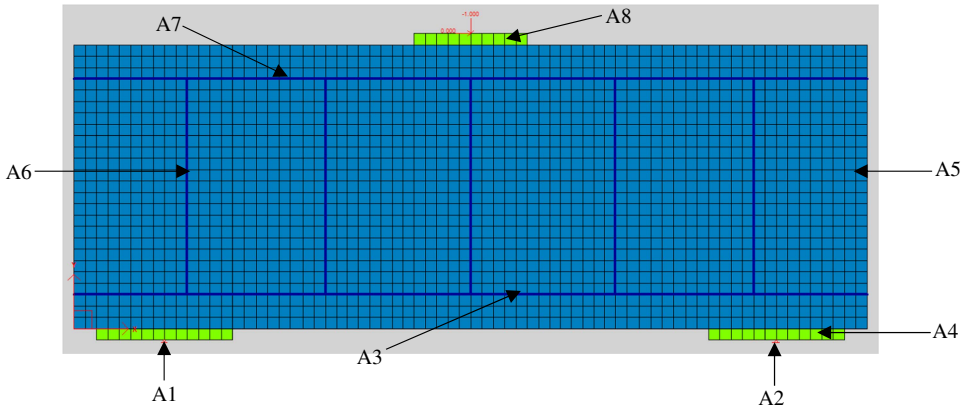

Fig. 14. Beam specimen.

Table 1. Finite-element material description

Label	Description
A1	Support condition (roller)
A2	Support condition (pin)
A3	Longitudinal reinforcing bars (2-10M or 2-15M)
A4	Structural steel plate on reaction
A5	Concrete material or steel-fiber reinforced concrete
A6	Shear reinforcement (D4)
A7	Hanger bar (2-10M reinforcing bars)
A8	Structural steel plate for load application

any given fatigue loading cycles. The values are used to modify the concrete strength and steel reinforcement ratios at a crack, and they include an accumulated fatigue prestrain and slip prestrain. Having accounted for the corresponding damage, the monotonic response is again obtained iteratively. This is repeated for given cycles until instability is reached.

Solutions for Fatigue Loading at 10,000 Cycles

Solution for Fig. 5 (Box 1)
Strain components after iterations are

$$\{\varepsilon\} = \begin{bmatrix} 0.584 \\ 1.278 \\ 2.604 \end{bmatrix} \times 10^{-3}; \qquad \{\varepsilon_c\} = \begin{bmatrix} 0.804 \\ 1.072 \\ 2.569 \end{bmatrix} \times 10^{-3}$$

The principal strains are estimated from $\{\varepsilon_c\}$ as follows:

$$\varepsilon_{c1} = 2.23 \times 10^{-3}; \qquad \varepsilon_{c2} = -0.353 \times 10^{-3}; \qquad \theta_\sigma = 42.02^0$$

Solution for Fig. 5 (Box 2): Average Stresses in Concrete and Reinforcement
Because the concrete is in a cracked state, Eqs. (20)–(22) are used for concrete compressive stress, and Eq. (35) is used for concrete tensile stress (neglecting the influence of steel fiber). The damage parameter required in the equation is obtained from Eqs. (29)–(31). The fatigue prestrain value [Eqs. (16)–(19)] is also required for estimating concrete compressive stress

$$f_{c2} = 5.34 \text{ MPa}$$

$$f_{c1} = 1.07 \text{ MPa}$$

Assuming a perfect bond between concrete and steel reinforcement, the average strain in the concrete is equal to the average strains in the steel reinforcing bars and the corresponding stresses

$$\varepsilon_{sx} = 0.584 \times 10^{-3}$$

$$\varepsilon_{sy} = 1.278 \times 10^{-3}$$

$$f_{sx} = E_s \varepsilon_{sx} = 117 \text{ MPa } (x\text{-direction})$$

Table 2. Description of specimens

Concrete batch	Volume of steel fiber, V_f (%)	Specimen identification number	Design f_c^d [MPa (ksi)]	ρ_l (%)	ρ_v (%)	Maximum fatigue load (% Pu)	Minimum fatigue load (% Pu)	Number of cycles to failure, N
2	0	C'S	50	0.9	0.2	Monotonic	—	—
2	0	CS	50	0.45	0.2	Monotonic	—	—
1	0	C'-70-0	50	0.9	0.2	70	1.3	210,000
1	0	C-80-0	50	0.45	0.2	80	1.8	47,000
3	0.75	A80-0F0.75	50	0.45	0.2	80	1.8	66,000
4	1.5	A80-0F1.5	50	0.45	0.2	80	1.8	320,000
1	0	C-70-0	50	0.45	0.2	70	1.8	72,000
3	0.75	A70-0F0.75	50	0.45	0.2	70	1.8	123,000
3	0	A70-0N0.75	50	0.45	0	70	1.8	260,000
4	1.5	A70-0F1.5	50	0.45	0.2	70	1.8	410,000
1	0	C'-80-0	50	0.9	0.2	80	1.3	62,000
5	1.5	B80-0N1.5	50	0.9	0	80	1.3	650,000

Note: V_f (%) = steel-fiber volume content; f_c^d = design compressive strength of concrete; ρ_l (%) = longitudinal reinforcement ratio; ρ_v (%) = shear reinforcement ratio; and Pu = ultimate load capacity.

Table 3. Fatigue life for beam specimens (experimental and predicted)

Specimen	Experiment load (kN)	Fatigue life (experiment) cycles, N_{fe}	NLFEA load, H_l (kN)	Predicted fatigue life, N_{fv} (NLFEA)	Predicted fatigue load, H_p (NLFEA)	NLFEA H_p/H_l	$\text{Log } N_{fv}/\text{log } N_{fe}$
C'-70-0	274	210,000	250	200,000	—	—	1.00
C'-80-0	312	62,000	275	60,000	—	—	0.98
C-70-0	192	72,000	180	60,000	—	—	0.98
C-80-0	219	47,000	196	40,000	—	—	0.99
A70-0F0.75	192	123,000	180	—	185	1.03	—
A80-0F0.75	219	66,000	196	—	200	1.02	—
A70-0F1.5	192	410,000	180	—	187	1.04	—
A80-0F1.5	219	320,000	196	—	200	1.02	—
A70-0N0.75	192	260,000	180	—	180	1.00	—
B80-0N1.5	312	650,000	275	—	275	1.00	—

$$f_{sy} = E_s \varepsilon_{sy} = 256 \text{ MPa } (y\text{-direction})$$

Solution for Fig. 5 (Box 3): Local Stresses at Crack

The local stresses are estimated from Eqs. (6) and (7) (neglecting the influence of steel fibers). In Eqs. (6) and (7), the reinforcement crack-growth factor (Zo) is estimated (indicated by the letter C in Fig. 5). The average reinforcement stresses are required in C to estimate the progressive crack depth

$$\varepsilon_{\text{scrx}} = 1.033 \times 10^{-3}; \qquad f_{\text{scrx}} = 207 \text{ MPa}$$

$$\varepsilon_{\text{scry}} = 1.642 \times 10^{-3}; \qquad f_{\text{scry}} = 300 \text{ MPa}$$

$$v_{ci} = 0.621 \text{ MPa}$$

Solution for Fig. 5 (Box 4): Crack Slip Strains

The slip at a given fatigue loading cycle can be calculated using Eq. (40). Subsequently, the shear strains (in x-y directions) resulting from slip at the crack are estimated. Fatigue irreversible compressive strain values are also evaluated in the x-y direction. The prestrain is equal to the summation of the shear strains. The pseudoload $[\sigma^o]$ is estimated from the obtained values of prestrain. The shear strain resulting from the crack slip is estimated as $\gamma_s = \delta_s/s = 0.429 \times 10^{-3}$; resolving into x- and y-components

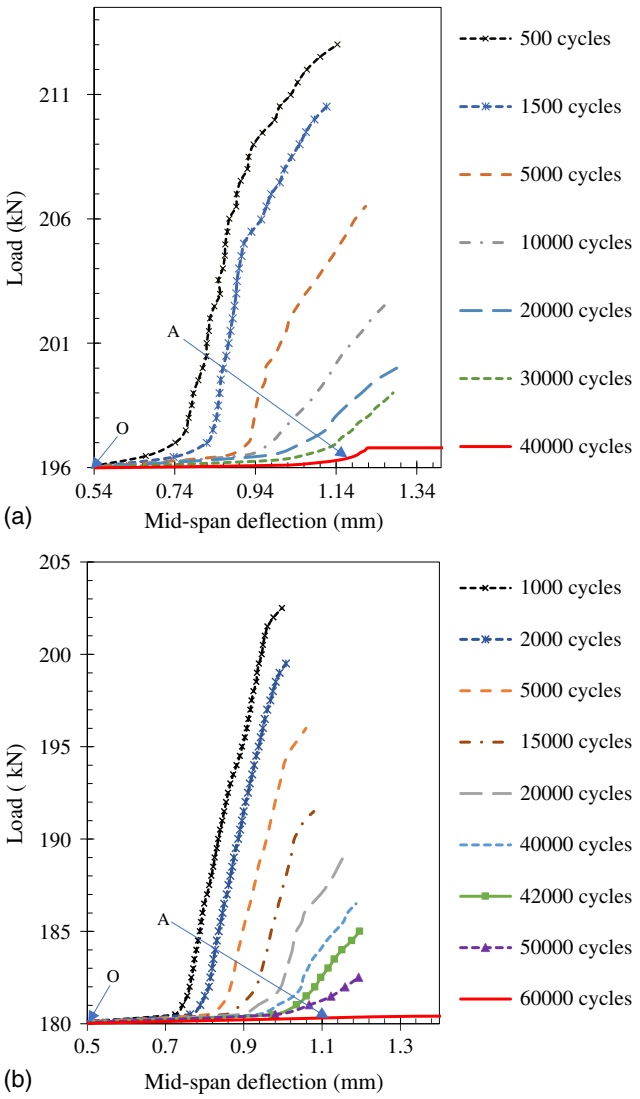

Fig. 15. Calculated fatigue residual capacity for (a) Beam C-80-0; and (b) Beam C-70-0.

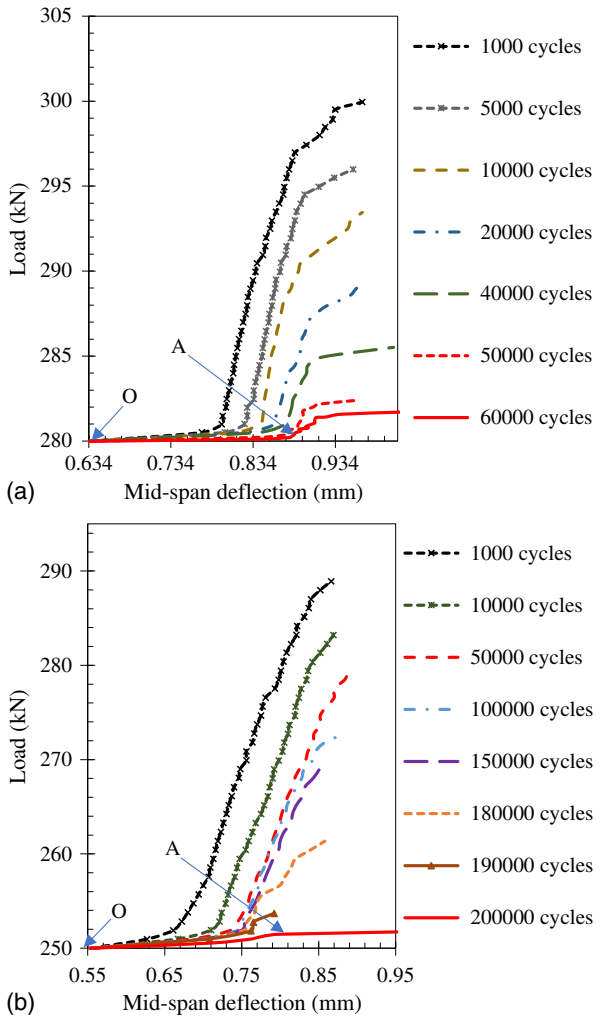

Fig. 16. Calculated fatigue residual capacity for (a) Beam C'-80-0; and (b) Beam C'-70-0.

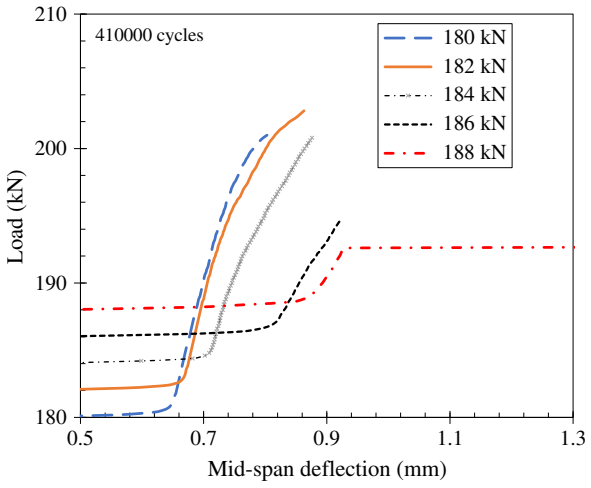

Fig. 17. Calculated fatigue residual capacity evolution for Beam A70-0F1.5.

$$\varepsilon_x^s = -\gamma_s/2 \cdot \sin 2\theta = -0.213 \times 10^{-3}$$

$$\varepsilon_y^s = \gamma_s/2 \cdot \sin 2\theta = 0.213 \times 10^{-3}$$

$$\gamma_{xy}^s = -\gamma_s/2 \cdot \cos 2\theta = 0.022 \times 10^{-3}$$

Inclusion of Irreversible Fatigue Strain as Offset Strain

$$\varepsilon_x^{\text{fat}} = \varepsilon_{c,2}^{\text{fat}}/2 \cdot (1 - \cos 2\theta) = -0.609 \times 10^{-5}$$

$$\varepsilon_y^{\text{fat}} = \varepsilon_{c,2}^{\text{fat}}/2 \cdot (1 + \cos 2\theta) = -0.750 \times 10^{-5}$$

$$\gamma_{xy}^{\text{fat}} = -\varepsilon_{c,2}^{\text{fat}}/2 \cdot \sin 2\theta = 0.135 \times 10^{-4}$$

Solution for Fig. 5 (Box 5): Material Secant Moduli

The net strain values are obtained from Eq. (12) (for concrete). The ratio of the average stress to net strain gives the secant modulus for concrete. In the case of steel reinforcement, the ratio of the average stress in steel reinforcement to the induced strain gives the secant modulus

$$E_{c1} = 480 \text{ MPa}$$

$$E_{c2} = 15{,}124 \text{ MPa}$$

$$G_c = 466 \text{ MPa}$$

$$E_{sx} = 200{,}000 \text{ MPa}$$

$$E_{sy} = 200{,}000 \text{ MPa}$$

Solution for Fig. 5 (Box 6): Material Stiffness Matrices $[D_c]$, $[D_s]$, and $[D]$

The stiffness matrices are obtained from Eqs. (51)–(55). The transformed composite stiffness matrix is obtained using Eq. (54). The transformed composite stiffness matrix at 10,000 cycles was obtained

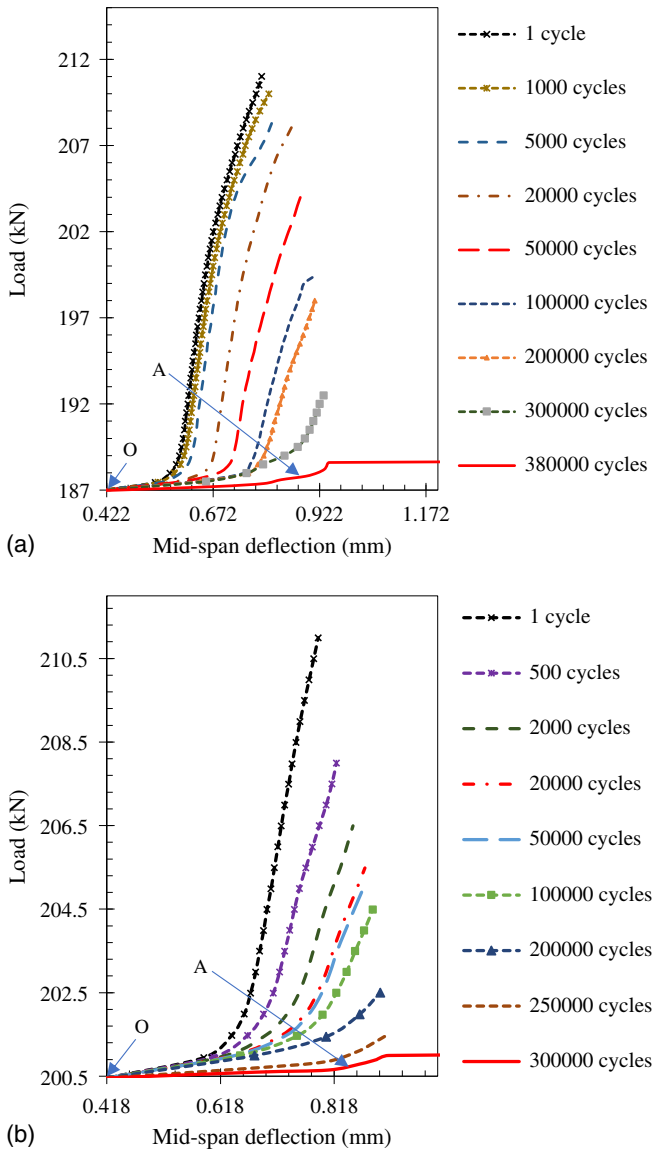

Fig. 18. Calculated fatigue residual capacity for (a) Beam A70-0F1.5; and (b) Beam A80-0F1.5.

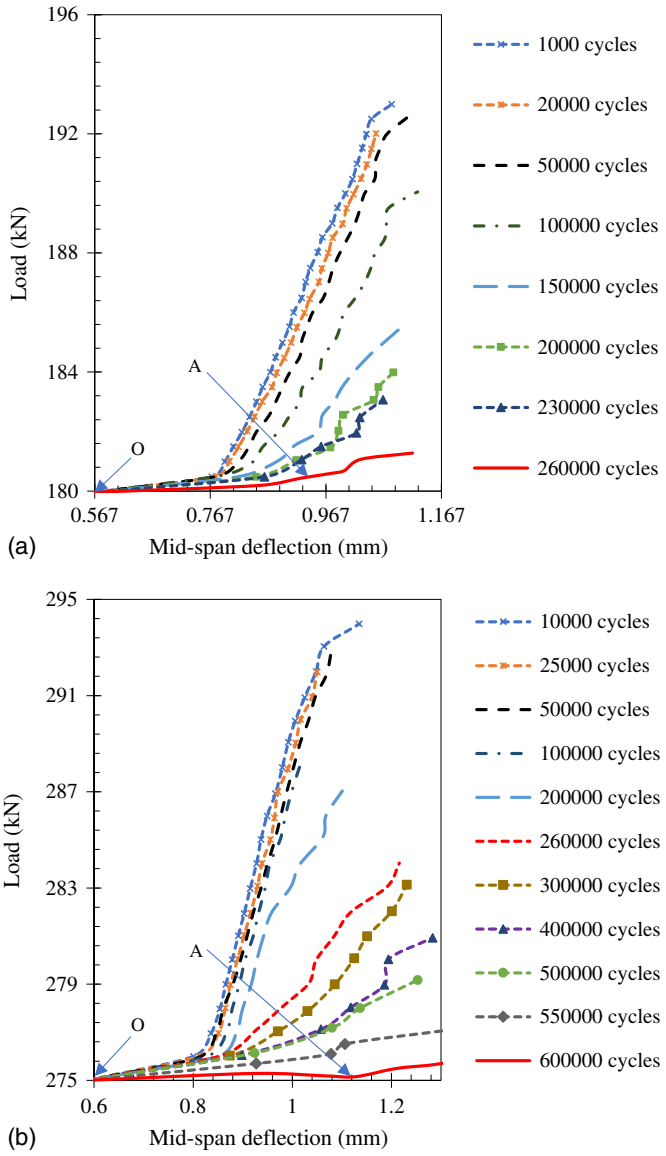

Fig. 19. Calculated fatigue residual capacity for (a) Beam A70-0N0.75; and (b) Beam B80-0N1.5.

$$[D] = \begin{bmatrix} 7{,}213 & 3{,}367 & -3{,}256 \\ 3{,}367 & 6{,}653 & -3{,}992 \\ -3{,}256 & -3{,}992 & 3{,}861 \end{bmatrix} \text{(MPa)}$$

Solution for Fig. 5 (Box 7): Determine Element Prestress Vector $[\sigma^o]$

The element prestress vector is calculated from Eq. (56). Herein, two prestrain values were considered: shear strain at crack and fatigue irreversible strain. The summation of the prestrains $[\varepsilon^0_{ps}]$ equals

$$\begin{bmatrix} -0.22 \\ 0.21 \\ 3.58 \end{bmatrix} \times 10^{-3}$$

$$[\sigma^o] = \begin{bmatrix} -0.13 \\ 0.26 \\ -5.35 \end{bmatrix} \text{ MPa}$$

Solution for Fig. 5 (Box 8): Determine New Estimates of Strain $\{\varepsilon\}$ and $\{\varepsilon_c\}$

The total and net strain values are estimated using Eq. (57). Because the results presented herein were obtained toward convergence, the final values were also equal to the initial values. However, where significant variations are observed, the iteration continues as illustrated using the given steps. This procedure was repeated as the number of fatigue loading cycles was increased.

At the final collapse or failure of a structural element (in this case, shear reinforcement in the vertical direction failed first), instability is observed and significant deformation persists. The results for the three different loads used are given in Figs. 7–12. They are presented in terms of the crack slip evolution, shear stress evolution, reinforcement crack depth propagation (in the y-direction where failure occurred), reinforcement strain, and stress evolutions.

From the results, the influence of fatigue load on fatigue life is well-captured as observed in all deformation evolution plots (Figs. 7–12). As the fatigue load increased, the corresponding fatigue life reduced, and the rates of deformation were observed to increase. In addition, the significance of the proposed approach stems from the fact that the profiles obtained in each case resembles the well-known fatigue deformation profile for reinforced concrete. Based on these observations, the deformation evolution within the cracked plane in reinforced concrete or steel-fiber concrete can be obtained using the proposed approach.

Finite-Element Modeling

The beam specimens shown in Fig. 13 were modeled with concrete or steel-fiber concrete, discrete reinforcement, and steel plates at the loading point and at the supports. The labels in the finite-element

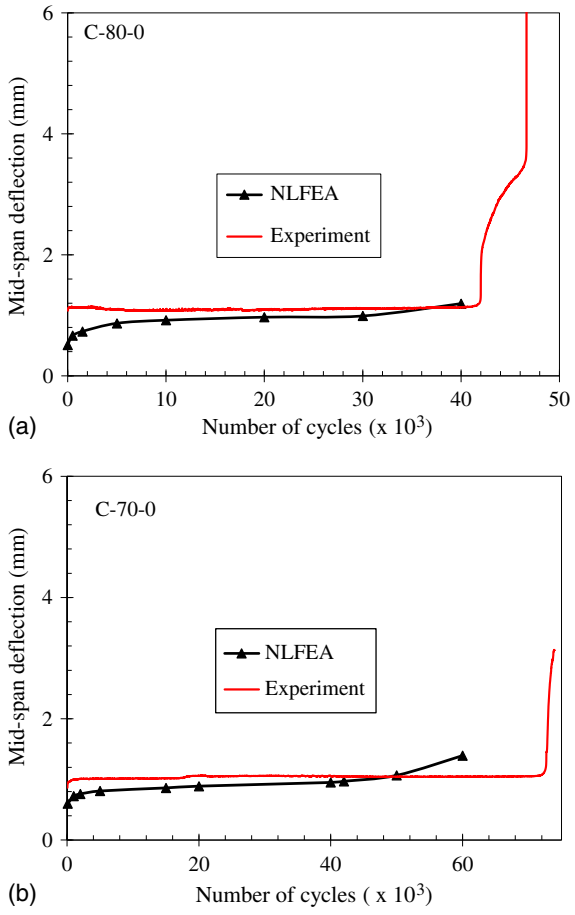

Fig. 20. Midspan deflection evolution for (a) C-80-0; and (b) C-70-0.

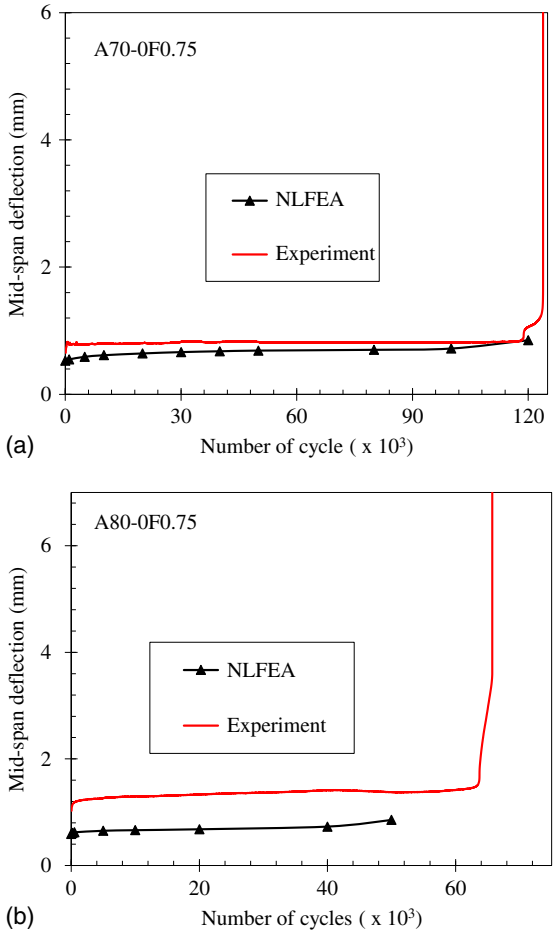

Fig. 21. Midspan deflection evolution for (a) A70-0.75; and (b) A80-0F0.75.

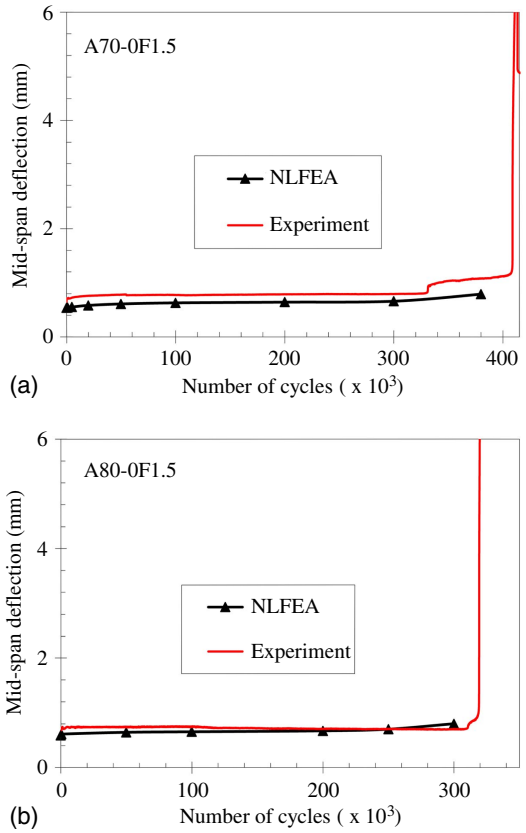

Fig. 22. Midspan deflection evolution for (a) A70-0F1.5; and (b) A80-0F1.5.

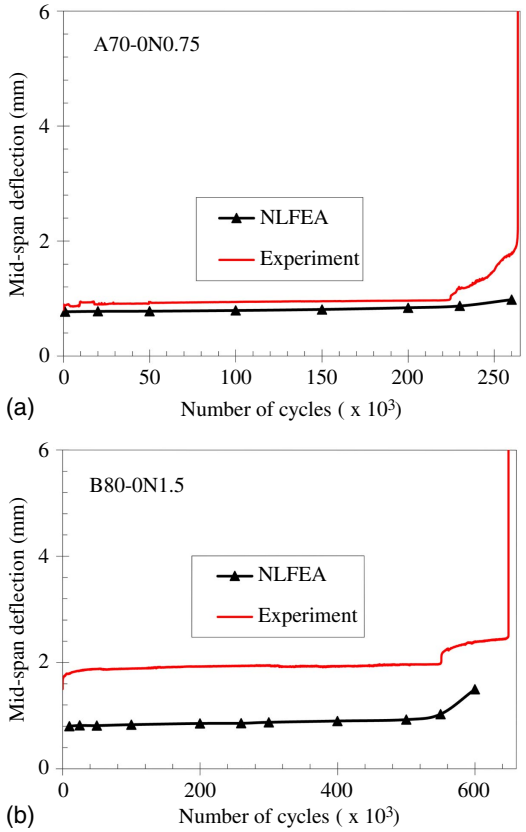

Fig. 23. Midspan deflection evolution for (a) A70-0N0.75; and (b) B80-0N1.5.

model shown in Fig. 14 are described in Table 1. A roller and a pin support were used to portray a simply supported beam.

Average compressive strengths of 59 and 55 MPa were used for conventional reinforced and steel-fiber reinforced concrete, respectively. Steel fiber volume ratios of 0.75% and 1.5% were used, and all beams were reinforced longitudinally with either two 15M or two 10M Canadian standard rebars. Some beams contained Canadian standard D4 (cold-worked, 5.5-mm diameter) shear reinforcing bars. The average yield strength values obtained for the 15M, 10M, and D4 bars were 430, 480, and 610, respectively.

The steel fibers used were high-strength end-hooked steel fibers (Dramix RC80/30BP, Zwevegem, Belgium) with an ultimate tensile stress capacity of 3,070 MPa. The residual flexural tensile strength ($F_{R,1}/F_{R,4}$) for steel fiber volume ratios of 0.75% and 1.5% from conducted experiments were obtained as 4.5/3.0 and 6.0/4.2, respectively (Vandewalle et al. 2003). Details of the beams tested in the reported experimental investigation are given in Fig. 13 and Table 2.

Based on experimental results, the cylinder strain corresponding to the compressive strength of plain concrete was taken as 2.1×10^{-3}, and the corresponding cylinder strain was approximately 3.0×10^{-3} for steel-fiber concrete volume ratios of $0.75V_f$ and $1.5V_f$. From the reported investigation, the monotonic resistance capacities of two beams reinforced longitudinally with 2-15M and 2-10M reinforcing bars were obtained as 390 and 270 kN, respectively (Isojeh et al. 2017b).

The monotonic response of the beams were also obtained using VecTor2 version 4.1 nonlinear finite-element analysis. For the beams reinforced with 2-15 M and 2-10 M reinforcing bars, resistance capacities of 350 and 250 kN were obtained, respectively.

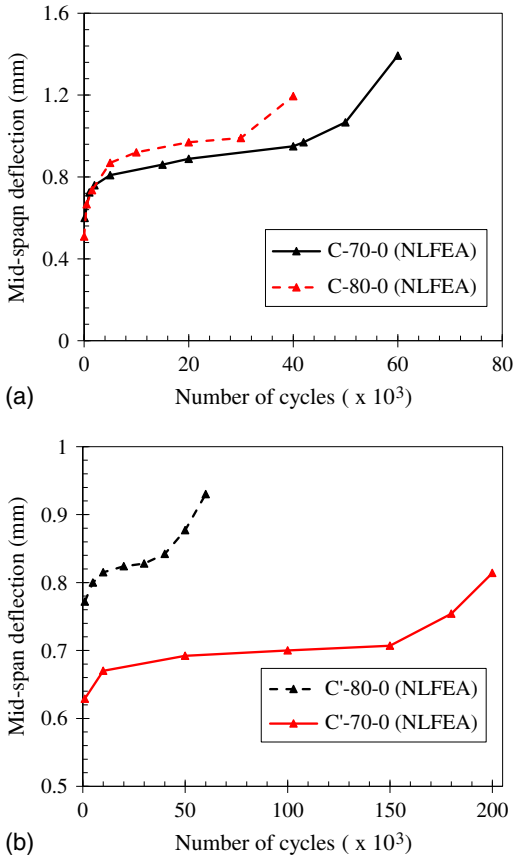

Fig. 24. Midspan deflection evolution (effect of stress level): (a) 10M bars; and (b) 15M bars.

Similar to the experimental procedures reported by Isojeh et al. (2017b), 80% and 70% of the capacities were used as fatigue loading on plain and steel-fiber reinforced concrete beams having the same longitudinal reinforcement ratio as each beam tested under monotonic load. Other fatigue loading parameters (as in experiment) include a sinusoidal waveform with a frequency of 5 Hz, and a minimum fatigue load of 5 kN in all cases (Column 8 of Table 2).

Average tensile strengths of steel-fiber concrete for 0.75% and 1.5% were approximately 3 and 4 MPa, respectively, based on experimental results. In the finite-element model, a perfect bond was assumed between steel reinforcement and the concrete composite. For fatigue loading, elasto-perfectly plastic models were used for the reinforcement.

For plain concrete, the Popovics and Popovics/Mander's constitutive models [Eqs. (23)–(26)] were implemented for compression prepeak and postpeak stress-strain relations, whereas for steel fibers, the models proposed by Lee et al. (2016) [Eqs. (27) and (28)] were used for compression prepeak and postpeak.

Fatigue Life and Deformation Evolution Predictions

The maximum fatigue load is mainly considered per fatigue load cycle in estimating the induced material stresses, and the influence of the minimum fatigue loading is accounted for using the load ratio parameter as indicated in the proposed damage models. The material stresses in all elements corresponding to the first load stage under monotonic loading are substituted into damage models (Fig. 5).

The predicted fatigue life corresponds to the number of cycles at which the resistance capacity of a beam reduces to a value approximately equal to the applied maximum fatigue load. The deformation (midspan deflection) at the second load stage is assumed to correspond to the deformation resulting from the applied fatigue loading cycles. The results of finite-element analyses of the specimens in Table 2 are presented in terms of fatigue residual capacity, midspan deflection evolution, and reinforcement stresses. The predicted fatigue life and fatigue loads are given in Table 3.

Fatigue Residual Capacity

Figs. 15 and 16 are the load-deformation plots for conventional reinforced concrete beams at different numbers of cycles. The number of cycles giving rise to each load-deformation plot, indicated by the letter A, corresponds to the fatigue life. The other plots at different fatigue loading cycles exhibit substantial but depreciating resistance capacities. Compared with the experimental results obtained for fatigue life, the fatigue life predictions obtained from the

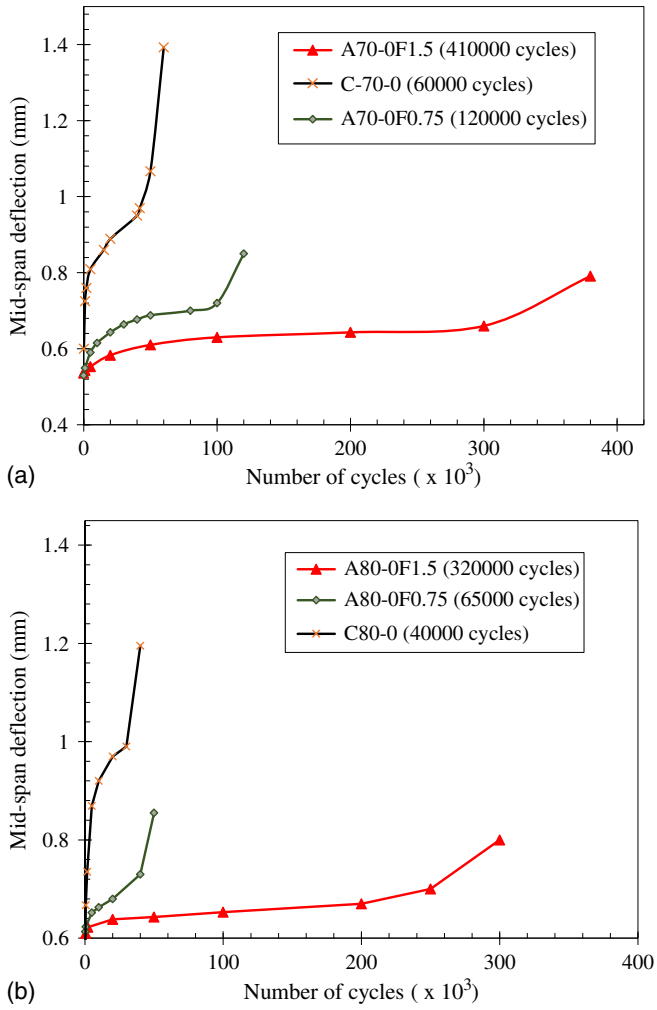

Fig. 25. Midspan deflection evolution (effect of steel fibers): (a) 70%; and (b) 80%.

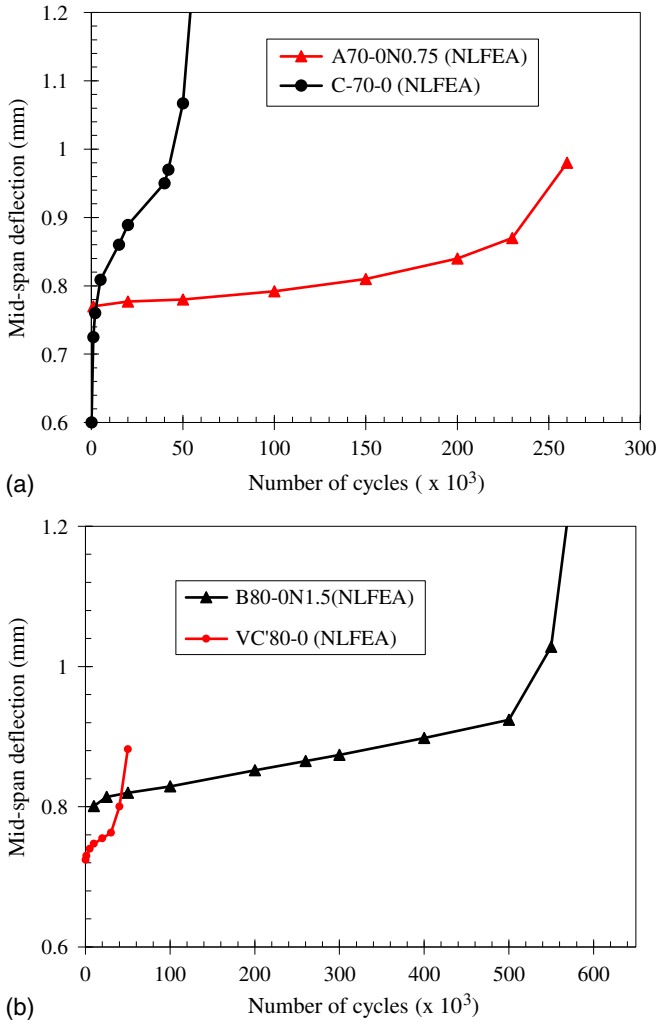

Fig. 26. Midspan deflection evolution (effect of steel fibers): (a) 70%; and (b) 80%.

nonlinear finite element analysis (NLFEA) are not only conservative, they portray good correlation.

In the case of the steel-fiber reinforced concrete beams, the approximate load that will result in the collapse of each modeled beam at the number of cycles resulting in failure obtained from the experiment was first predicted. In Fig. 17, as the maximum fatigue load was increased from 180 to 188 kN (at 410,000 cycles for Beam A70-0F1.5), the residual capacity reduced. Subsequently, load-deformation plots for increments in the number of cycles at the predicted loads were obtained. The residual capacities are given in Figs. 18 and 19. The predicted fatigue load for each steel-fiber reinforced concrete beam is reasonably close to the actual fatigue load of 80% and 70% of the monotonic resistance capacity of corresponding control beams from NLFEA. Therefore, the responses from conventional reinforced and steel-fiber reinforced concrete can be compared for beams having similar loading parameters.

The results are also presented in Table 3. Table 3 provides the ratio of the calculated fatigue load to the actual fatigue loads corresponding to 70% or 80% of the undamaged beam resistance capacities obtained from NLFEA. The ratio of the logarithm of predicted fatigue life (using VecTor2) to the experimental fatigue life can also be seen in Table 3. As observed in both cases, the predictions are of good accuracy; however, the predictions for steel-fiber reinforced concrete beams fatigue load from NLFEA reveal a slight underestimation of the fatigue damage.

Midspan Deflection Evolution

The midspan deflection evolution for the beams modeled in VecTor2 are shown in Figs. 20–23. The evolutions obtained from the experimental results are also included. Although the predicted evolving values from NLFEA tend to be slightly lower, overall,

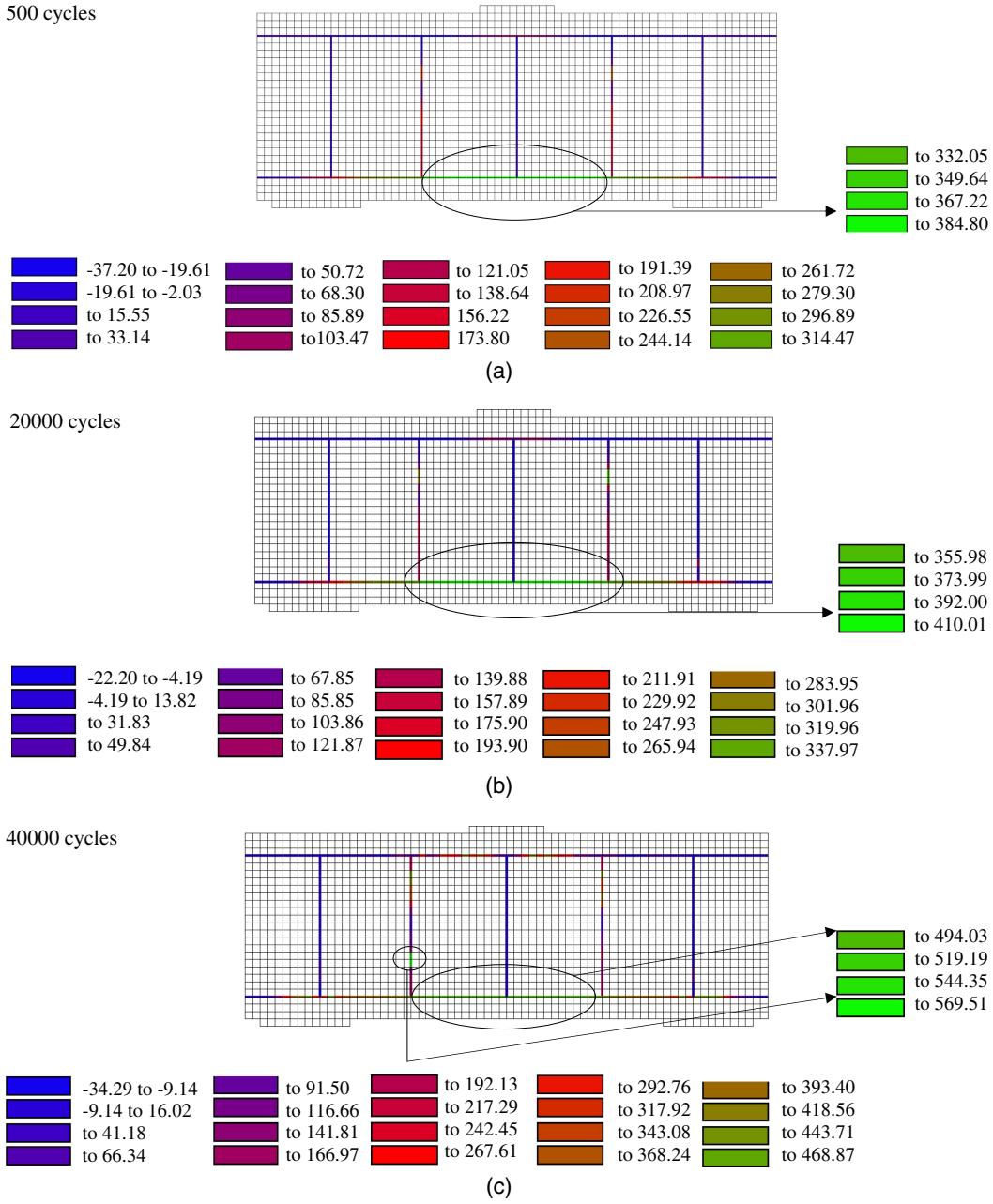

Fig. 27. Evolution of stresses in reinforcing bars for Beam C-80-0.

the validation of the experimental results (midspan deflection evolution) with the predicted results are of acceptable accuracy. The predicted evolution profiles are shown in a subsequent section for variations in loading and material parameters.

Variations in Loading and Material Parameters

As shown in Fig. 24, as the fatigue load increases from 70% to 80% of the monotonic resistance capacity, the fatigue life was observed to reduce. In addition, the deformations (midspan deflection) and corresponding rate of evolution were also observed to increase.

From Fig. 25, the increase in fatigue life as steel fiber volume ratio increases from 0 to 1.5% was well-captured using the VecTor2 NLFEA software (based on the proposed fatigue-damage algorithm). In addition, from NLFEA predictions (Fig. 26), like experimental results, steel-fiber reinforced concrete beams without shear reinforcement resulted in enhanced fatigue life compared to conventional reinforced concrete beams. However, higher initial deflections were observed in the former because they were less stiff.

Reinforcement Stresses under Fatigue Loading

To illustrate the steel reinforcement stress evolution, plots of the steel reinforcement stresses at given fatigue loading cycles were obtained as shown in Figs. 27 and 28.

The local stresses in the reinforcement at a concrete crack location after 500, 20,000, and 40,000 cycles are given in Figs. 27(a–c). The probable region of fracture (where the induced stress is equal to yield) is shown in Fig. 27(c) at 40,000 cycles. Reinforcement stresses (shear and longitudinal) within the same region in Figs. 27(a and b) at 500 and 20,000 cycles are lower than the yield value. However, the stresses evolve progressively as the number of fatigue loading cycles increase. From the figures, failure was observed to be attributable to

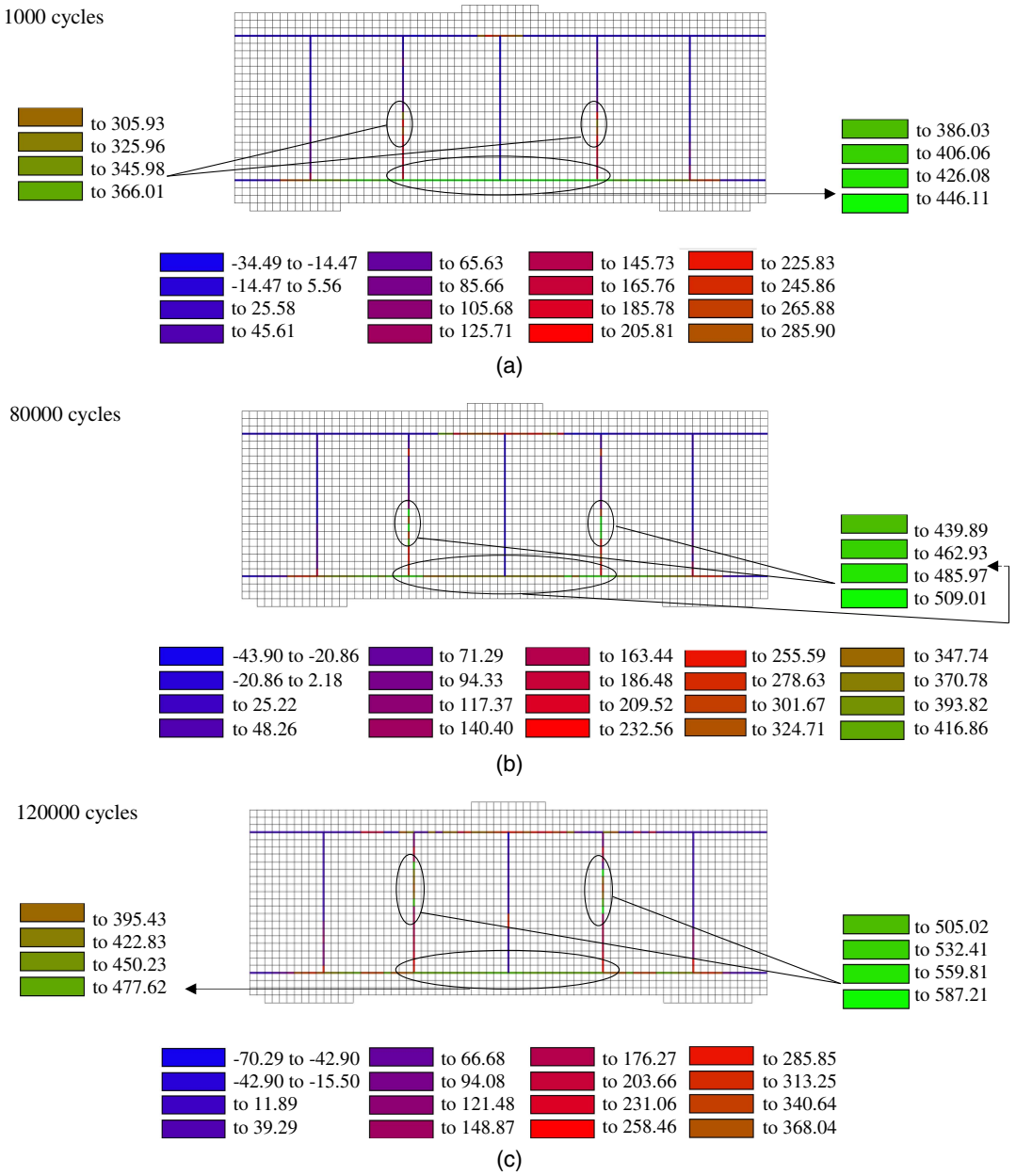

Fig. 28. Evolution of stresses in reinforcing bars for Beam A70-0F0.75.

fracture of longitudinal reinforcement. Similar observations are shown in Fig. 28.

Variable Fatigue Loading

In practice, the fatigue loading of reinforced concrete structures is usually variable in nature and not constant. In the experimental investigation conducted and validated herein, constant fatigue loading was used. The approach described also considers constant fatigue loading. Two approaches for variable fatigue loading are discussed subsequently.

Most designers still prefer the use of the Palmgren-Miner damage rule based on simplicity. Variable fatigue loads, and the corresponding number of cycles applied, are usually given in spectrums. The proposed approach (using NLFEA) can be used to estimate the number of cycles leading to failure (N_f) for each fatigue load in the spectrum, and the ratio of N to N_f is obtained for each fatigue load in the spectrum. Hence, the Palmgren-Miner rule may be used to cumulate the expected damage. The flaw of negligence in the loading sequence and the effect of previous damage consideration has reduced the reliability of this approach. Better still, an equivalent cycle concept may be used for the fatigue analysis of reinforced concrete structures under variable fatigue loading. Using Fig. 29, this approach is discussed.

The load-deformation plots of all variable loads are obtained using the proposed approach and assuming a constant fatigue load for each. For simplicity, the midspan deflection evolution plots for Beams C-70-0 and C-80-0 subjected to two different loads (70-0 and 80-0) are used for this illustration. Assuming a beam is subjected to N_1 cycles (load of 80-0), in Fig. 29, the corresponding midspan deflection is δ_1. For a second variable load (70-0) subjected to N_2 cycles, the effect of the first variable load must be accounted for. Hence, δ_1 is extended to the load-deformation plot for the second variable load, and the corresponding number of cycles is termed the equivalent cycles (N_{equiv}) (Fig. 29). To obtain the actual deflection (δ_2) due to N_2 having considered the damage from the first load stage, the summation of N_{equiv} and N_2 ($N_{\text{equiv}} + N_2$) is extended to the load-deformation plot for the second variable load. This procedure is repeated for subsequent variable loads until the critical point on the last load-deformation plot is reached (Cr_i). For more fatigue loads, the procedures continue. This approach accounts for previous loading damage; hence, it overcomes the sequence and load history anomaly common with variable fatigue loading.

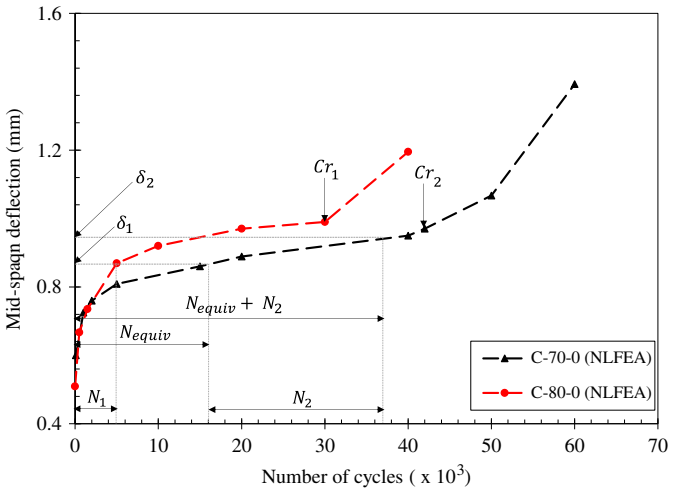

Fig. 29. Variable fatigue loading of reinforced concrete.

Conclusions

An algorithm was described for implementing damage models for concrete strength and stiffness, irreversible strain accumulation, and steel reinforcement crack growth in a finite-element analysis framework. This procedure was then implemented into the disturbed stress field model for fatigue analysis of reinforced concrete and steel-fiber structures. Fatigue-damage models that account for salient loading parameters and appropriate evolution models for concrete parameters were introduced. As an improvement to reported models, the implementation of the reinforcement crack-growth model and concrete damage models account for the progressive deformation and shear transfer at a crack under fatigue loading for reinforced concrete and steel-fiber reinforced concrete. It is proposed that the fatigue life of a structural component corresponds to the number of fatigue loading cycles at which the resistance capacity degrades to a value equal to the fatigue load. Verification of the proposed algorithm and fatigue failure criterion with conducted experimental results was required to ascertain its validity. Corroborated results using nonlinear finite-element analysis gave a good correlation.

Acknowledgments

The authors gratefully acknowledge the Natural Science and Engineering Research Council (NSERC) of Canada and Hatch Ltd. for the invaluable contributions and financial support to this research. The authors also acknowledge the assistance received from the Niger Delta Development Commission and the Delta State Government of Nigeria.

Notation

The following symbols are used in this paper:

a, b, c = material parameters;
C = material constant = 2×10^{-13};
C_f = frequency factor;
D = damage;
D_c = concrete stiffness matrix;
D_s = reinforcement stiffness matrix;
D_{cr} = critical damage;
D_{ft} = concrete tensile strength damage;
D_{te} = concrete tensile secant modulus damage;
d_{bi} = rebar diameter;
E_c = elastic modulus of concrete;
E_{c1} = secant modulus in tension;
E_{c2} = secant modulus in compression;
E_s = elastic modulus of steel reinforcement;
f = frequency;
$f_{c,\text{TS}}$ = average tensile stress in concrete due to tension stiffening effect;
f_{cx} = normal stress in concrete in horizontal direction;
f_{cy} = normal stress in concrete in vertical direction;
f_{c1} = effective tensile stress of concrete;
f_{c2} = effective compressive stress of concrete;
$f_{c2\max}$ = peak compressive stress in concrete considering compression softening effect;

f_c' = compressive strength of concrete;
f_c^* = degraded compressive strength;
f_{eh} = tensile stress due to mechanical anchorage effect of end-hooked steel fiber;
f_f = tensile stress at crack due to steel fiber;
f_p = initial compressive strength;
f_{scri} = local stress in reinforcement at crack;
$f_{s,i}$ = average stress in steel reinforcement;
f_{st} = tensile stress due to frictional bond behavior of steel fiber;
f_t = residual tensile strength of concrete;
f_t^* = degraded strength at which concrete cracks;
f_{tp} = initial concrete tensile strength;
G_c = shear modulus;
k = postdecay parameter for stress-strain response of concrete in compression;
N = number of cycles;
N_f = numbers of cycles at failure;
N_{ij} = interval of cycles considered;
n = material constant = 3;
s_{cr} = crack spacing;
T = period of fatigue cycle;
t_d = direction coefficient (= 0.6 or 1.0);
V_f = steel fiber volume ratio;
v_{cxy} = shear stress in concrete in horizontal direction;
v = Poisson's ratio;
v_{ci} = shear stress;
$v_{ci,cr}$ = shear stress at cracked concrete plane;
w_{cr} = crack width;
α_{avg} = coefficient to relate tensile stress at a crack due to steel fibers with average tensile stress;
α_i = inclination of reinforcement;
β = material constant;
β_2 = material constant;
Δ = deformation;
$\Delta\varepsilon_{1cr}$ = change in strain at crack;
δ_s = crack slip;
ε_{c1} = net tensile strain;
ε_{c2} = net compressive strain;
ε_c^* = strain corresponding to the degraded compressive strength;
ε_p = initial strain corresponding to the initial compressive strength;
$\varepsilon_{\text{scri}}$ = local strain in the reinforcement;
$\varepsilon_{s,i}$ = average strain in steel reinforcement;
ε_{1cr} = local strain at crack;
γ_s = shear strain due to crack slip;
θ, θ_c = inclination of principal strain direction;
θ_f = angle between tensile stress direction due to steel fibers and principal tensile stress direction in concrete;
θ_{ni} = angle between the reinforcement direction and the normal to the crack; and
ρ_i = reinforcement ratio.

References

Aas-Jacobsen, K. 1970. *Fatigue of concrete beams and columns*. Bulletin No 70-1. Trondheim, Norway: Institutt for Betonkonstruksjoner.

Collins, M. P., and D. Mitchell. 1997. *Prestressed concrete structures*. Woodbridge, Canada: Copywell.

Deluce, J. R., S. C. Lee, and F. J. Vecchio. 2014. "Crack model for steel fiber-reinforced concrete members containing conventional reinforcement." *ACI Struct. J.* 111 (1): 93–102.

Dowling, N. E., and S. Thangjitham. 2000. *An overview and discussion of basic methodology for fatigue*. ASTM STP 1389. West Conshohocken, PA: ASTM.

Eligehausen, R., M. Kazic, and T. M. Sippel. 1992. "Creep and fatigue analysis of reinforced concrete structures." In *Proc., Int. Conf. on Bond in Concrete from Research to Practice*, 7-49–7-58. Riga, Latvia: Riga Technical Univ.

Facconi, L., G. Plizzari, and F. J. Vecchio. 2014. "Disturbed stress field model for unreinforced masonry." *J. Struct. Eng.* 140 (4): 04013085. https://doi.org/10.1061/(ASCE)ST.1943-541X.0000906.

Gao, L., and C. T. T. Hsu. 1998. "Fatigue of concrete under uniaxial compression cyclic loading." *ACI Mater. J.* 95 (5): 575–581.

Grebreyouhannes, E., T. Kishi, and K. Maekawa. 2008. "Shear fatigue of cracked concrete interface." *J. Adv. Concr. Technol.* 6 (2): 365–376.

Hanson, J. M. 1983. "Design for fatigue." In *Handbook of structural concrete*, edited by F. K. Kong, et al., 35. London: Pitman.

Hognestad, E. 1957. "Confirmation of inelastic stress distribution in concrete." *J. Struct. Div.* 83 (2): 1–17.

Holmen, J. O. 1982. "Fatigue of concrete by constant and variable amplitude loading." *ACI Spec. Publ.* 75 (4): 71–110.

Isojeh, B., M. El-Zeghayar, and F. J. Vecchio. 2017a. "Concrete damage under fatigue loading in uniaxial compression." *ACI Mater. J.* 114 (2): 225–235.

Isojeh, B., M. El-Zeghayar, and F. J. Vecchio. 2017b. "Fatigue behavior of steel fiber concrete in direct tension." *J. Mater. Civ. Eng.* 29 (9): 04017130. https://doi.org/10.1061/(ASCE)MT.1943-5533.0001949.

Isojeh, B., M. El-Zeghayar, and F. J. Vecchio. 2017c. "Fatigue resistance of steel-fibre reinforced concrete deep beams." *ACI Struct. J.* 114 (5): 1215–1226. https://doi.org/10.14359/51700792.

Isojeh, B., M. El-Zeghayar, and F. J. Vecchio. 2017d. "Simplified constitutive model for fatigue behavior of concrete in compression." *J. Mater. Civ. Eng.* 29 (7): 04017028. https://doi.org/10.1061/(ASCE)MT.1943-5533.0001863.

Isojeh, M. B., and F. J. Vecchio. 2016. "Parametric damage of concrete under high-cycle fatigue loading in compression." In *Proc., 9th Int. Conf on Fracture mechanics of Concrete and Concrete Structures*. Bayonne, France: IA-FRAMCOS.

JSCE (Japan Society of Civil Engineers). 1986. *Standard specification for design of concrete structures*. Tokyo: JSCE.

Lee, S. C., J. Y. Cho, and F. J. Vecchio. 2013. "Tension-stiffening model for steel fiber-reinforced concrete containing conventional reinforcement." *ACI Struct. J.* 110 (4): 639–648.

Lee, S. C., J. Y. Cho, and F. J. Vecchio. 2016. "Analysis of steel fibre-reinforced concrete elements subjected to shear." *ACI Struct. J.* 113 (2): 275–285. https://doi.org/10.14359/51688474.

Lovegrove, J. M. 1981. "Stress intensity factors for fatigue cracking of round bars." *Int. J. Fatigue* 3 (3): 117–123. https://doi.org/10.1016/0142-1123(81)90059-1.

Maekawa, K., K. Toongoenthong, E. Gebreyouhannes, and T. Kishi. 2006. "Direct path-integral scheme for fatigue simulation of reinforced concrete in shear." *J. Adv. Concr. Technol.* 4 (1): 159–177. https://doi.org/10.3151/jact.4.159.

Miner, M. A. 1945. "Cumulative damage in fatigue." *J. Appl. Mech.* 12 (1): A159–A164.

Oh, B. H. 1991. "Cumulative damage theory of concrete under variable-amplitude fatigue loadings." *ACI Mater. J.* 88 (2): 122–128.

Okamura H., S. A. Farghaly, and T. Ueda. 1981. "Behaviour of reinforced concrete beams with stirrups failing in shear under fatigue loading." In Vol. 308 of *Proc., Japan Society of Civil Engineers*, 109–122. Tokyo: JSCE.

Otter, D. E., and A. E. Naaman. 1986. "Steel fibre reinforced concrete under static and cyclic compressive loading." In *Proc., 3rd RILEM Symp. on Developments in Fibre Reinforced Cement and Concrete*. Paris: RILEM.

Otter, D. E., and A. E. Naaman. 1988. "Properties of steel fibre reinforced concrete under cyclic loading." *ACI Mater. J.* 85 (4): 254–261.

Palmgren, A. 1924. "Die Lebensdauer von Kugellagern." *Zeitschrift des Vereines Deutscher Ingenieure* 68 (14): 339–341.

Park, Y. J. 1990. "Fatigue of concrete under random loadings." *J. Struct. Eng.* 116 (11): 3228–3235. https://doi.org/10.1061/(ASCE)0733-9445(1990)116:11(3228).

Petryna, Y. S., D. Pfanner, F. Stangenberg, and W. B. Kratzig. 2002. "Reliability of reinforced concrete structures under fatigue." *Reliab. Eng. Syst. Saf.* 77 (3): 253–261. https://doi.org/10.1016/S0951-8320(02)00058-3.

Popovics, S. 1973. "A numerical approach to the complete stress strain curve for concrete." *Cem. Concr. Res.* 3 (5): 583–599. https://doi.org/10.1016/0008-8846(73)90096-3.

Socie, D., N. E. Dowling, and P. Kurath. 1984. "Fatigue life estimation of notched members." In *Proc., Fracture Mechanics: Fifteenth Symp.*, 284–299. West Conshohocken, PA: ASTM.

Tamulenas, V., V. Gelazius, and R. Ramanauskas. 2014. "Calculation technique for stress-strain analysis of RC elements subjected to high-cycle compression." *Civ. Transp. Eng. Aviation Technol.* 6 (5): 468–473.

Teng, S., and F. Wang. 2001. "Finite element analysis of reinforced concrete deep beams under fatigue loading." *ACI Struct. J.* 98 (3): 315–323.

Tilly, G. P., and D. S. Moss. 1982. "Long endurance fatigue of steel reinforcement." In *Proc., Fatigue of Steel and Concrete Structures Colloquium*, 229–238. Lausanne, Switzerland: International Association for Bridge and Structural Engineering.

Torrenti, J. M., G. Pijaudier-Cabot, and J. Reynouard. 2010. *Mechanical behavior of concrete: Cyclic and dynamic loading, fatigue of structural concrete*, 185–223. Hoboken, NJ: John Wiley & Sons.

Vandewalle, L., et al. 2003. "RILEM TC 162-TDF: 'Test and design methods for steel fiber reinforced concrete'-sigma-epsilon method-final recommendation." *Mater. Struct.* 36 (262): 560–567.

Vecchio, F. J. 2000. "Disturbed stress field model for reinforced concrete: Formulation." *J. Struct. Eng.* 127 (1): 1070–1077. https://doi.org/10.1061/(ASCE)0733-9445(2000)126:9(1070).

Vecchio, F. J. 2001. "Disturbed stress field model for reinforced concrete: Implementation." *J. Struct. Eng.* 127 (1): 12–20. https://doi.org/10.1061/(ASCE)0733-9445(2001)127:1(12).

Vecchio, F. J., and M. P. Collins. 1986. "The modified compression field theory for reinforced concrete elements subjected to shear." *J. Am. Concr. Inst.* 83 (2): 219–231.

Vecchio, F. J., and D. Lai. 2004. "Crack shear-slip in reinforced concrete elements." *J. Adv. Concr. Technol.* 2 (3): 289–300. https://doi.org/10.3151/jact.2.289.

Vega, I. M., M. A. Bhatti, and W. A. Nixon. 1995. "A nonlinear fatigue damage model for concrete in tension." *Int. J. Damage Mech.* 4 (4): 362–379. https://doi.org/10.1177/105678959500400404.

Xiang, T., and R. Zhao. 2007. "Reliability evaluation of chloride diffusion in fatigue damaged concrete." *Eng. Struct.* 29 (7): 1539–1547. https://doi.org/10.1016/j.engstruct.2006.09.002.

Zanuy, C., L. Albajar, and P. Fuente. 2009. "Sectional analysis of concrete structures under fatigue loading." *ACI Struct. J.* 106 (5): 667–677.

Zhang, B., D. V. Phillips, and D. R. Green. 1998. "Sustained loading effect on the fatigue life of plain concrete." *Mag. Concr. Res.* 50 (3): 263–278. https://doi.org/10.1680/macr.1998.50.3.263.

Zhang, B., D. V. Phillips, and K. Wu. 1996. "Effects of loading frequency and stress reversal on fatigue life of plain concrete." *Mag. Concr. Res.* 48 (177): 361–375. https://doi.org/10.1680/macr.1996.48.177.361.